Learning alters theta-nested gamma oscillations in inferotemporal cortex

Keith M Kendrick[1], Yang Zhan[1], Hanno Fischer[1] Ali U Nicol[1] Xuejuan Zhang[2] & Jianfeng Feng[3]

[1]Cognitive and Behavioural Neuroscience, The Babraham Institute, Cambridge, CB22 3AT, UK

[2]Mathematics Department, Zhejiang Normal University, Jinhua 321004, Zhejian Province, PR China

[3]Department of Computer Science, Warwick University, Coventry CV4 7AL UK and Centre for Computational Systems Biology, Fudan University, Shanghai, PR China.

Corresponding authors:

keith.kendrick@bbsrc.ac.uk

jianfeng.feng@warwick.ac.uk

How coupled brain rhythms influence cortical information processing to support learning is unresolved. Local field potential and neuronal activity recordings from 64-electrode arrays in sheep inferotemporal cortex showed that visual discrimination learning increased the amplitude of theta oscillations during stimulus presentation. Coupling between theta and gamma oscillations, the theta/gamma ratio and the regularity of theta phase were also increased, but not neuronal firing rates. A neural network model with fast and slow inhibitory interneurons was developed which generated theta nested gamma. By increasing N-methyl-D-aspartate receptor sensitivity similar learning-evoked changes could be produced. The model revealed that altered theta nested gamma could potentiate downstream neuron responses by temporal desynchronization of excitatory neuron output independent of changes in overall firing frequency. This learning-associated desynchronization was also exhibited by inferotemporal cortex neurons. Changes in theta nested gamma may therefore facilitate learning-associated potentiation by temporal modulation of neuronal firing.

The functions of both low and high frequency oscillations in the brain have been the subject of considerable speculation[1]. Low frequency theta oscillations (4-8Hz) have been observed to increase in terms of power and phase-locked discharge of single neurons in a visual memory task[2]. In hippocampus the phase of theta rhythm functions as the clock signal for timing of pyramidal neurons and long-term potentiation (theta peaks) and depotentiation (theta troughs)[3]. These findings may reflect the patterns of synaptic plasticity and maintenance of the memory for a stimulus. Fast frequency gamma oscillations (30-70Hz) can provide tighter control and coordination than oscillations in a lower frequency range[4]. Thus gamma activity in local neural circuits is hypothesised to be responsible for higher cognitive functions such as perceptual binding of visual features[5]. Studies of human electroencephalographic (EEG) recordings show event-related gamma activity indicating gamma as a signature of cortical

networks underlying object representations[6]. Recent examples of coupling between gamma amplitude and theta phase (theta-nested gamma)[7] therefore provide an effective combination for neuronal populations to communicate and integrate information during visual processing and learning and may provide a process of temporal segmentation that can maintain multiple working memory items[8]. Modulation of oscillatory synchronization can also increase synaptic gain at postsynaptic target sites thereby potentiating responses to learned stimuli[9-10].

There is still debate as to whether critical changes in theta or gamma involve amplitude or phase parameters, or both. Some human EEG recording studies have reported that theta phase rather than amplitude is correlated with cognitive processes, the so-called phase reset model[1,11], while others in the frontal and temporal lobes have placed more importance on the correlation between theta amplitude and gamma frequency[7]. The magnitude of both theta and gamma oscillations during encoding also appears to predict the efficacy of subsequent recall[12] and the theta rhythm can both modulate gamma amplitude[13] and the firing of single neurons[2]. We have investigated the impact of learning on theta and gamma oscillatory activity in the inferotemporal cortex (IT) of three sheep, using 64-electrode recording arrays, while the animals performed a face or object-pair discrimination learning paradigm[14]. We then developed a neural network model reproducing our electrophysiological findings to infer the functional consequences of observed learning associated changes.

RESULTS

Theta and gamma oscillations are coupled in inferotemporal cortex

Overall data was collected from 17 recording sessions (5-6 per sheep) and during presentation of 20 face (5-10 per sheep) and 2 non-face object pairs (one each in 2 sheep)(see **Supplementary Fig. 1** online). There were no systematic differences in the patterns of theta or gamma oscillations in response to the different types of stimuli and so data were combined.

A wavelet transform applied to each individual LFP showed substantial theta band activity across the 4-8Hz range, and synchronised across IT electrodes, before and during stimulus presentation (see **Supplementary Fig. 2** online). There was a much smaller contribution from gamma band activity (30-70Hz) and across the recording sessions there was significant ($P<0.001$) coupling between theta phase and gamma amplitude before (mean±sem = 76.5±6.2% of recording electrodes in left IT and 84.6±4.2% in right IT) and during (80.6±5.8% in left IT and 84.6±4.7% in right IT) visual stimulus presentation (see **Fig. 1a**).

Since our data confirmed the presence of cross-frequency coupling between theta and gamma oscillations, similar to that reported in human EEG studies[7], we investigated whether the correlation between theta phase and gamma amplitude was a consequence of theta nested-gamma activity. To test this, we generated one theta wave and gamma wave and nested (added) them together using two sine waves of 5 Hz and 50 Hz which were linearly mixed. The gamma frequency sine wave (50 Hz) had an amplitude 1/5th of the theta frequency one (5Hz). Using a trial length of 500 ms, 30 trials were generated with a sampling frequency of 1 kHz. White noise was then added to the mixed sine waves with a signal to noise ratio equal to -5 dB. The coherence between the theta phase and gamma amplitude was maximal (**Fig. 1b**) confirming that the relationship between the theta phase and gamma amplitude is indeed a consequence of theta nested-gamma activity.

Learning increases theta amplitude, theta/gamma coupling and the theta/gamma ratio

An analysis of theta wave activity revealed a significant increase in the amplitude and power of the first theta wave after stimulus onset which was enhanced ~1.5 fold following learning (**Fig. 2b** and **Supplementary Table 1** online). The proportion of recording electrodes showing a significant ($P<0.05$) rise in theta amplitude and power increased in all animals after learning and in both left and right IT (mean±sem Sheep A: Right 5.5±4.7% before

learning vs 72.9±9.3% after learning, t-test two-tailed, $t^{15} = -7.3$, $P<0.001$; Sheep B: Left 5.7±2.7% vs 52±8.7% $t^{22} = -4.04$, $P<0.001$, Right 7.8±5.6% vs 59±11.8% $t^{20} = -3.41$ $P = 0.002$; Sheep C: Left 0% vs 32.6±9.2%, using one-sample t-test , $t^{6} = 3.55$ $P = 0.012$, Right 0% vs 61.5±16.2%, $t^{6} = 3.79$ $P = 0.009$). No individual electrodes showed a significant increase in gamma amplitude and power although there was a small overall significant increase across electrodes following learning in the right IT of one animal (**Fig. 2c**). The net result was a significant ~1.4 fold increase in the ratio of theta to gamma during stimulus presentation after learning (**Fig. 2d**). Coupling between theta and gamma was also strengthened after learning in terms of a greater coherence (~10%) between the two frequencies (**Fig. 2e**) together with a tightening of theta phase, although with the latter only in the right IT where z-scores for theta phase were ~3-fold higher than in the left IT (**Fig. 2f**).

We found no evidence for theta-phase resetting in response to stimulus presentation with <1.5% of recording electrodes showing a significant ($P<0.05$) effect. There was also no significant increase in the associated phase reset z-score following learning (**Fig. 2g**).

Overall, levels of theta synchronization across recording electrodes were higher in the right hemisphere (>95%) than in the left (47-48%) but with no effect of learning (**Fig. 2h**). This together with the theta phase-tightening our results indicates a greater degree of synchronization in theta activity in the right compared with the left IT, although it is high in both hemispheres. Such hemispheric differences might reflect a greater synchronization of synaptic inputs to the right IT from earlier centres in the visual processing system.

Learning does not alter stimulus evoked visual potentials or neuronal firing rates

Following stimulus onset there were similar peak response latencies for the visual evoked potential (VEP – characterised by P100 and N300 components see **Fig. 2a**), MUA and first theta wave (overall mean±sem across all recording sessions across the 3 animals: VEP: P100

= Right 129±7 ms, Left = 118±6 ms; N300 = Right 366±13 ms Left 324±16 ms; MUA: Right 267±4 ms, Left 255±4 ms; Theta = Right 257±14 ms, Left 231±11 ms) (see **Fig. 2a**). Neither the response latencies nor the magnitudes of the P100 and N300 components of VEPs were influenced by learning (data not shown). While the magnitude of MUA responses changed significantly in response to stimuli both for electrodes with overall increased (overall mean±sem pre = 17±1.1Hz vs during = 29.4±1Hz before learning, t^4 = -18.4, P<0.001 and 19.7±1.7Hz vs 31.6±1.8Hz after learning, t^4 = -37.6, P<0.001) or decreased activity (pre = 29.2±1.5Hz vs during = 17.1±1Hz before learning, t^4 = 15.7, P<0.001 and 32±2Hz vs 19.7±1.2Hz after learning, t^4 = 16.0, P<0.001) there was no significant effect of learning on this or on the proportion of electrodes showing increased firing rates (48.4±2.5% vs 52.1±3.5%, t^4 = -1.62, P = 0.18). This is therefore consistent with the absence of learning-associated changes in gamma amplitude.

Learning-evoked changes in theta/gamma activities can occur in <10 min

The learning effects on IT theta nested gamma could be extremely rapid and with two face pairs, from two different animals, we were able to plot changes across sequential blocks of trials taking place over 20-30 min where learning was successfully achieved. In both cases there was a very close correspondence between the attainment of the >80% learning criterion and the changes in theta amplitude the theta/gamma ratio and coherence (see **Fig. 3**). In three other cases (2 face pairs and 1 object pair) where learning only occurred after a number of days of training there was also a similar close relationship between the achievement of the >80% learning criterion and altered theta amplitude, theta/gamma ratio and coherence values. Overall for the five different stimulus pairs when comparisons were made between the trials during learning and the first 40 trials where learning was achieved there was an enhancement in the IT of the stimulus-evoked increase in theta amplitude (mean±sem change from pre

(100%) to during stimulus = 106.8±4.1% during learning vs 124.9±2.7% after learning, paired t-test, $t^4 = -3.07$, P=0.04), the theta/gamma ratio (113.6±10.7% vs 132.5±6.7%, $t^4 = -2.97$, P=0.04), theta/gamma coherence (105.5±3.7% vs 119.4±5%, $t^4 = -2.89$, P=0.04) and theta phase tightening (only for right IT, 101.7±2.4% vs 107.8±3.4%, $t^4 = -5.14$, P=0.007).

Theta-nested gamma can be generated by neuronal networks incorporating both fast and slow inhibitory interneurons

We next generated a neural network model based on 100 excitatory (glutamatergic with α-amino-3-hydroxyl-5-methyl-4-isoxazole-propionate (AMPA) and N-methyl-D-aspartatic acid (NMDA) receptors) output neurons modulated by 50 fast and 50 slow inhibitory (γ-aminobutyric acid type A receptors ($GABA_A$) neurons and projecting to a single downstream neuron (see **Fig. 4a**). By adjusting the coupling strength between these neurons we found they could indeed produce theta-nested gamma oscillations (**Fig. 4b**). The generation of theta nested gamma required only a weak, but present, coupling coefficient between the fast inhibitory $GABA_A$ receptor type neurons and the excitatory ones and a strong coupling between the latter and the slow inhibitory type ones. There also had to be recurrent coupling between the fast inhibitory and excitatory cells. Increasing the fast inhibitory coupling strength tended to amplify gamma activity whereas increasing that of the slow inhibitory coupling amplified theta. So the two types of connections appear competitive in this context.

Learning effects on theta/nested gamma in the model are produced by altering NMDA receptor sensitivity and potentiate responses by downstream neurons

We first established that the model was able to reproduce patterns of theta and gamma activities observed in the IT. Simulations revealed similar changes in theta power during stimulus application and at the same latency (see **Supplementary Figs 2 & 3** online). Theta

activity was also strongly synchronised and there was phase tightening during the stimulus (see **Supplementary Figs 4 & 5** online).

Having validated the model's utility we next used it to investigate potential functional consequences of shallow nested gamma (as seen after learning) on communication between excitatory and downstream neurons in comparison with deeper nested gamma (similar to before learning) or where gamma activity was minimal. **Fig. 4b** shows that the downstream neuron response during the stimulus is strongest when there is shallow nested gamma and there is increased theta amplitude and strong coupling between the two frequencies. With deeper nested gamma, excitatory neuron responses appear more highly synchronised and there is reduced theta/gamma coherence and a weaker downstream neuron response. When gamma is minimised there is also reduced downstream neuron activity and theta/gamma coherence (**Fig.4b**). Thus for optimal coupling between gamma and theta, and to evoke maximal responses in the downstream neuron, gamma should be shallow nested on theta as seen after learning.

We then used the model to investigate if NMDA receptor changes alone in the network could reproduce learning-induced changes in IT theta/gamma activity. It was found that increased NMDA receptor sensitivity on and between the excitatory neurons (NMee) and between them and the slow inhibitory ones (NMes) could account for the enhanced theta amplitude without changing gamma (**Fig 5a**). It was possible to achieve the same outcome by combining NMDA receptor changes with increased $GABA_A$ receptor sensitivity between the slow inhibitory and excitatory neurons (data not shown). If the connection with the fast inhibitory neurons (NMef) was also altered this increased gamma amplitude and therefore did not replicate IT findings. Changes in the theta gamma ratio and theta/gamma coherence seen in IT recordings were also confirmed (**Figs 5b,c**). Theta and gamma amplitude and

coherence values were higher in the model than in IT recordings although the theta/gamma ratio was similar. This probably reflects the limited network size and complexity of the model compared with the IT itself and the greater noise inherent in *in vivo* brain recordings. **Figs 5d,e** show that firing rates of the excitatory neurons are slightly decreased following the NMDA receptor changes mimicking learning but there is nevertheless a highly significant overall increase in the firing rate of the downstream neuron and this is positively correlated with the size of the theta/gamma ratio (Pearson correlation, $r = 0.34$, $P<0.01$ – **Fig. 5f**).

Both the model and IT recordings show temporal desynchronization of neuronal output occurs following learning induced theta-nested gamma changes

The potentiation of downstream neuron responses predicted by the model despite the absence of excitatory output neuron firing rate changes suggests that some form temporal re-organisation of the latter is occurring to enhance their impact. We therefore investigated whether temporal synchronization in the excitatory neuron output to the downstream neuron is significantly altered as a result of simulated learning changes. Repeated simulations using the model confirmed that learning produced a significantly greater desynchronization of the excitatory neuron output across a range of stimulus strengths (overall mean ± sem synchronization index before learning = 0.068±0.0005 and after learning = 0.062±0.001 t-test, $t^{18} = -5.3$, $P<0.0001$, **Fig. 6a**). Synchronization levels were negatively correlated with the size of the theta/gamma amplitude ratio (Pearson correlation $r = -0.42$, $P<0.001$, **Fig. 6b**) and the firing frequency of the downstream neuron ($r = -0.88$, $P<0.001$, **Fig. 6d**).

An analysis of the distribution of active excitatory neurons in the network revealed that activity occurred primarily during the peak and subsequent fall of each theta wave and that on average significantly more time bins contained firing neurones after changes associated

with learning (mean ± sem = 4.99±0.29 before learning vs 5.92±0.19 after learning, 5ms bins during each theta wave for 1s during the stimulus, $t^{18} = -2.73$, P=0.01, **Figs. 6 d and e**)

Our model therefore predicted that learning-induced changes in theta and its relationship to gamma should increase the impact of the firing of excitatory neurons on downstream ones by desynchronizing their output. We therefore investigated whether such desynchronization occurred in MUA recordings from IT neurons. Despite the contribution of both inhibitory interneurons and output neurons to the MUA, after learning there was indeed a significant desynchronization across the 5 electrode arrays in the 3 animals during the period of the first theta wave after stimulus onset (during learning synchronization index = 0.0867±0.007 pre-stimulus and 0.0905±0.009 during stimulus, t-test, $t^4 = -0.9$, P = 0.42; after learning = 0.0856±0.005 vs 0.0797±0.006, $t^4 = 4.41$, P= 0.01). This difference between during and after learning was significant (% change from baseline (100%) during stimulus = 104.3±4.7% during- vs 94.2±1.4% after learning, paired t-test $t^4 = 2.71$ P=0.05). As in the model, levels of synchronization were also negatively correlated with the theta/gamma ratio (Pearson correlation, r = -0.29, P<0.001, **Fig 6c**) and after learning there were significantly more 5ms bins with spike activity across each electrode during stimulus period theta waves (4.30±0.28 vs 4.93±0.22, $t^4 = -4.75$, P=0.009 using only electrodes showing stimulus-evoked increased firing rates in the recording arrays, **Supplementary Fig 6** online). There was also a significant negative correlation between the number of bins with spike activity per theta wave and the magnitude of the synchronization index (r = - 0.3, P = 0.01).

DISCUSSION

Overall therefore our results have demonstrated for the first time that theta nested gamma in the IT is both influenced by learning and may serve an important function in the amplification and discriminability of inputs converging onto downstream neurons through a

temporal desynchronization effect. These learning effects can also be extremely rapid (<10 min). The shallow-nested coupling of theta and gamma frequencies is essential for this functional outcome with learning induced changes in theta amplitude rather than theta phase being of key importance. Our neural network model also demonstrates for the first time that competitive and reciprocal coupling between fast and slow inhibitory interneurons and excitatory output ones is important for the production of theta-nested gamma and that learning-induced changes within the IT can be simulated simply by increasing NMDA receptor sensitivity within the proposed network as in many other learning situations.

To the best of our knowledge this is the first demonstration of the presence of theta-nested gamma in IT and our model shows that it could be maintained with a simple network of excitatory glutamatergic pyramidal neurons and slow and fast inhibitory $GABA_A$ receptor interneurons that could be present in this and other neocortical regions. That both slow and fast inhibitory interneurons are required for the generation of theta-nested gamma confirms a previous prediction[15], although differs from another study in the hippocampus suggesting that it is the h-current generated in oriens-lacunosum interneurons that is important[16]. The presence of such fast and slow type $GABA_A$ receptor responses has recently been confirmed in the neocortex[17] as well as the hippocampus[18].

The main learning-associated change in theta oscillations we found in the IT was in terms of amplitude rather than phase and our results therefore do not support a key role for resetting of theta phase in cortical information processing contrary to some previous studies[1,11]. The lack of any co-incident alteration in the amplitude of gamma oscillations is in-line with our similar failure to find any change in stimulus-evoked neuronal firing rates in the IT following learning. Indeed, previous research in monkeys has also failed to find evidence for reward-associated learning changes in firing rates of individual IT neurons[19].

While the effects on theta-nested gamma we observe following learning could be achieved by altering the sensitivity of NMDA receptors alone in our model they could also be reproduced through a combination of changes to both NMDA and $GABA_A$ receptors although it was felt that restricting changes to NMDA receptors alone more closely reflected known effects of learning induced plasticity changes in the brain where it is changes in NMDA receptors rather than in GABAergic ones that are consistently important[20].

A recent study has reported a decorrelation shift in visual cortex neurons during responses to visual stimuli using a pair-wise correlation analysis approach[21]. However, the greater desynchronization of neuronal activity we have observed following learning using a synchronization index measure across a whole network might still at first seem counter-intuitive. The increased theta amplitude we have shown, together with increased coherence between theta phase and gamma amplitude and a tightening of theta phase at individual electrodes, or the excitatory neurons in the model might indicate a tighter control of neuronal output and greater synchronization. However, changes in theta activity would also modulate the firing thresholds of the output neurons cells and the large increases seen after learning across the network would therefore result in a greater variability in firing thresholds. This would lead to a greater variability in the timings of firing thresholds being reached and an overall reduction in synchronisation with individual neurons becoming less likely to fire at the same time. Our findings from both the model and MUA showing that after learning there is neural spike activity across a wider range of time bins during theta waves in the stimulus period provides some support for this hypothesis.

The prediction from the model that the impact of increased desynchronization in IT output neurons would lead to enhanced responses by downstream target neurons might also seem counter-intuitive. However, the more synchronized are the outputs from excitatory neurons

converging onto a downstream neuron then the more input information can potentially be lost when more excitatory post synaptic potentials (EPSPs) are generated at the same time than are necessary to cause the downstream neuron to fire. However, if the EPSPs generated are more separated in time then they can avoid being rendered impotent by refractory period limitations and contribute more efficiently towards eliciting responses by the downstream neuron. Thus the net effect of a desynchronization shift in the IT output network could be that that the same number of EPSPs generated at downstream neurons would produce an enhanced response as observed in our model.

It would clearly be difficult to test the above model prediction directly *in vivo* without being able to make simultaneous recordings from multiple connected neurons in say IT and the frontal cortex. However, our combined *in vivo* and model simulation findings do provide a mechanism for how learning induced changes in theta-nested gamma could modulate temporal aspects of neuronal firing in neocortical networks such that downstream networks exhibit potentiated responses.

METHODS

Animals and visual discrimination training. Three female sheep were used (Ovis aries, one Clun Forest and two Dorsets). All experiments were performed in strict accordance with the UK 1986 Animals Scientific Procedures Act and during them the animals were housed inside in individual pens. The animals were trained initially over several months to perform operant-based face (sheep) or non-face (objects) discrimination tasks with a choice being made between two simultaneously presented pictures (side by side) only one of which was associated with a food reward. The position (left or right) of the rewarded picture was randomised in each trial. During stimulus presentations animals stood in a holding trolley and indicated their choice of picture by pressing one of two touch panels located in the front of

the trolley. The food reward was delivered automatically to a hopper between the two panels. The life-sized pictures were back projected onto a screen 0.5m in front of the animal using a computer data projector. A white fixation spot was presented constantly in between trials to maintain attention and experimenters waited until the animals viewed this spot before triggering presentation of the image pairs. The stimulus images remained in view until the animal made an operant response (generally around 1-3 s). In each case successful learning of a face or object pair required that a performance criterion of >80% correct choice over 40 presentation trials was achieved consistently. By the end of training animals were normally able to reach the >80% correct criterion after 40-80 learning trials and to maintain this performance. Some previously learned stimulus pairs (over periods ranging from 10 days to 9 months) were then presented during subsequent electrophysiological recording experiments although the animals were mainly presented with novel stimulus pairs and neurophysiological parameters recorded before and after the learning criterion was achieved.

For each sheep recordings were made in response to up to 11 different face or non face object pairs (Sheep A: 5 novel face and 1 novel object pair; B 7 novel face pairs, 3 previously learned face pairs and one previously learned object pair; Sheep C: 2 novel face pairs and 3 previously learned face pairs. Learning effects were monitored over between 80-189 trials and data was collected over blocks of 20-40 trials. For the face pairs Sheep A and B were discriminating between the faces of different socially familiar or unfamiliar individuals (face identity discrimination) whereas for Sheep C discrimination was between calm and stressed face expressions in the same animal (n=3 pairs) or in different animals (n=2 pairs). With this animal the calm face was the rewarded stimulus. Where novel face or object pairs were being learned during recordings the >80% performance criterion was normally achieved between 20 and 80 training trials. The face and object pairs used for each of the 3 sheep are shown in **Supplementary Fig. 1**.

Electrophysiology. Following initial behavioral training sheep were implanted under general anesthesia (fluothane) and full aseptic conditions with either unilateral (one animal) or bilateral planar 64-electrode (for configuration see **Supplementary Fig. 3a**) arrays (epoxylite coated, etched, tungsten wires with 250μM spacing – total array area ~2mm x 2mm, electrode impedance ~0.2MΩ) aimed at the IT. Holes (0.7cm diameter) were trephined in the skull and the dura beneath cut and reflected. The electrode bundles were introduced to a depth of 20-22 mm from the brain surface using a stereotaxic micromanipulator and fixed in place with dental acrylic and stainless-steel screws attached to the skull. Two of these screws acted as reference electrodes, one for each array. Electrode depths and placements were calculated with reference to X-rays, as previously described[22]. Electrodes were connected to 34 pin female plugs (2 per array) which were cemented in place on top of the skull (using dental acrylic). Starting 3 weeks later the electrodes were connected via male plugs and ribbon cables to a 128 channel electrophysiological recording system (Cerebus 128 Data Acquisition System - Cyberkinetics Neurotechnology Systems Inc., USA) and recordings made during performance of the different face and non-face pair operant discrimination tasks. This system allowed simultaneous recordings of both neuronal spike and local event-related (LFP) activity from each electrode. Typically, individual recording sessions lasted around 30 min and for 80-200 individual trials. There was at least a week between individual recording sessions in each animal.

The LFPs were sampled at 2 kHz and MUA spikes at 30 kHz and digitized for storage from ~3 seconds prior to the stimulus onset to ~3 seconds after the stimulus onset (stimulus durations were generally 1-3 s). Neural recordings from our data acquisition system consisted of two large raw data files, one for the LFP and the other for the MUA. We used

custom Spike 2 (Cambridge Electronic Design, Cambridge, UK) scripts to translate these into text files arranged either by trial or electrode prior to further analysis.

LFP or MUA data contaminated with noise artefacts, such as from animal chewing food, were excluded as were LFPs with unexpectedly high power. For LFPs, offline filtering was applied in the range of 1-200 Hz and trend was removed before spectral analysis. Any trials having more than 5 points outside the mean ± 5 standard deviation range were discarded before the analysis. Blocks of trials where no visual evoked potential could be discriminated (this only occurred in Sheep C) were also excluded. The mean and the standard deviation values of different parameters were calculated across all trials for 500 ms before and 500 ms during the presentation of the visual discrimination pairs (i.e. prior to the performance of any operant response). The LFPs and MUA responses were all aligned to the onset of the visual stimuli. All analyses were carried out using custom written routines in Matlab (The Mathworks Inc, Natick, MA). Use of custom spike-sorting software revealed that 1-4 single neurons were contributing to the MUA at each electrode[23].

At the end of the experiments animals were euthanized with an intravenous injection of sodium pentobarbitone and the brains removed for subsequent histological confirmation of X-rays that array placements were within the IT cortex region.

Visual evoked potentials (VEP) and MUA. The VEP was extracted from the LFPs by trial-averaging after aligning the data to the onset of stimulus. Two major peaks were identified from the VEP in the initial 500ms of stimulus presentation: positive peak at ~100ms (P100) and a negative peak at ~300ms (N300). We calculated the latency for these two peaks by finding the time corresponding to the maximum and minimum peak value respectively. The amplitudes of these two peaks were calculated as their peak values after subtracting the average baseline in the 100ms before stimulus onset.

For the analysis of MUA data a Gaussian kernel with width of 30ms was convolved to the spike train. We used the maximum peak value in the initial 500 ms of stimulus presentation to characterise the MUA latency. In each trial the responsive MUA was defined by a paired t-test ($P<0.05$) comparing the spike count in the pre-stimulus period and during-stimulus period using a bin width of 20 ms.

Time-dependent spectrum analysis. To extract spectral content relating to time, we used a wavelet transform to disclose the time-dependent spectrum of the LFP data. The wavelet transform convolves the LFP $x(t)$ with a mother wavelet $\psi(t)$ [24]:

$$CWT_x(t, f) = \sqrt{\frac{f}{f_0}} \int_{-\infty}^{\infty} x(\tau)\psi^*(\frac{\tau - t}{f_0} f)d\tau$$

Here we use Morlet wavelet f_0=0.849 defined as

$$\psi(f) = \pi^{1/4}\sqrt{2}\exp\{-\frac{1}{2}(2\pi f - 2\pi f_0)^2\}$$

The wavelet transform was applied to each individual LFP trial at each electrode and a final time-dependent spectrum estimated as the trial-averaged scalograms (modulus square of the wavelet transform). When comparing pre-stimulus and during stimulus theta band activity we used the amplitude of the wavelet transform at 4-8 Hz and averaged it across this band. For the gamma band amplitude in the 30-70Hz frequency range was analysed. Theta and gamma power was also calculated, although in our freely behaving animals we found the amplitude measure to be less variable across trials and sessions whereas power was susceptible to abrupt changes making comparisons more difficult. To determine the significance of responsiveness at each electrode a *post-hoc* t-test (with Benjamini-Hochberg correction) was used to compare the amplitude of the wavelet transform in the 500ms pre-stimulus with the 500ms during stimulus periods. The amplitude changes illustrating the effect of learning

were normalized by subtracting the amplitude value of the pre-stimulus period and dividing by the maximal value for each electrode.

The theta/gamma ratio was also calculated as the direct ratio between the theta amplitude and gamma amplitude (or theta power and gamma power).

Cross-frequency coupling. We used coherence analysis to measure the dependency between the signals in the two different frequency bands. The main idea of coherence analysis is to detect the modulation between amplitude and phase of the two band-limited signals in each frequency band. To do this we can separate the raw signal into two sets of band-pass filtered signals[25]. The first set has frequencies from 30 Hz to 70 Hz, in 2 Hz step with 1 Hz bandwidth. This will create a real-valued band-pass filtered signal set $\{x_{amplitude}(t)\}$ in which we can extract the amplitude signal used for gamma band. The second set of real-valued band-pass filtered signals $\{x_{phase}(t)\}$ is created by filtering the raw signal with centre frequencies from 2 Hz to 20 Hz, in 1 Hz step with 1 Hz bandwidth. This set can be used to extract the phase signal for the theta band. The amplitude and phase signals can be extracted by applying a Hilbert Transform to both sets to generate complex-valued analytic band-passed signals, i.e. $\{x_{amplitude}(t)\}$ is taken to create a set of analytic amplitude time series $\{A(t)\}$ and the phase set $\{x_{phase}(t)\}$ is extracted to create a set of analytic phase time series $\{\varphi(t)\}$. When we have both the amplitude and phase signals the coherence $C_{A^i(t)\varphi^j(t)}(f)$ between i-th amplitude signal A(t) and j-th phase signal $\varphi(t)$ is calculated by:

$$C_{A^i(t)\varphi^j(t)}(f) = \left| \frac{S_{A^i(t)\varphi^j(t)}(f)}{S_{A^i(t)A^i(t)}(f) S_{\varphi^{ji}(t)\varphi^{ji}(t)}(f)} \right|^2$$

Where $S_{A^i(t)A^i(t)}(f)$ and $S_{\varphi^{ji}(t)\varphi^{ij}(t)}(f)$ are the auto-spectra for the i-th A(t) and j-th $\varphi(t)$ and $S_{A^i(t)\varphi^j(t)}(f)$ is the cross-spectrum between them. The confidence interval for the coherence is given by[7]:

$1-\alpha^{1/(K-1)}$

where α is the significant level (e.g. $\alpha = 0.01$) and K is the trial number which corresponds to the disjointed number of periodograms. The phase-locking index is then measured by the coherence in the range between 0 and 1 so that a large coherence value indicates a strong cross-frequency modulation. Coherence calculation is attained at all the pair-wise frequency combinations between two bands and a Bonferroni correction is applied to the multiple comparisons over all the frequency pairs. The coherence analysis was performed for all the electrodes and at each electrode the theta/gamma coherence values were calculated for all the pairs in the theta and gamma band.

Phase reset. Since the complex Morlet wavelet was used to compute the time-dependent spectrum of LFP, the wavelet transform also provided phase information in the time-frequency domain. We therefore took out the angle of the complex wavelet transform as the instantaneous phase of LFP at each frequency. For a given trial k at time t the phase time series $\varphi_k(t)$ were obtained by wavelet-transforming the LFP in trial k. If an electrode exhibits phase-locking across N trials the distribution of phase should depart from uniformity and this can be tested by a Rayleigh statistic[25,26]:

$$R(t) = \frac{1}{N}\sqrt{\sum_{k=1}^{N}\cos\varphi_k(t) + \sum_{k=1}^{N}\sin\varphi_k(t)}$$

Therefore the hypothesis of uniformity should be rejected at a certain significance level if phase-locking was found for that electrode. The Z-score for the Rayleigh statistic is given as $Z = NR^2$.

To see if theta band waves exhibit phase-resetting with a locked phase over trials, we calculated the Z -scores as a function of time in the during-stimulus range across all trials. An electrode was considered to be phase-locking if all the samples from the time of stimulus onset at a given frequency (4 - 8Hz) pass the criterion of the Rayleigh test ($P < 0.001$) throughout two full oscillatory cycles. A comparison was made across all the electrodes in a recording array and a Bonferroni correction applied to compensate for type-I errors.

Cross-array synchronization. To assess whether there was synchronization of the LFP phases, the Rayleigh statistic was also used to calculate a Z-score across all the electrodes. In each trial the Z-score for theta phase (4-8Hz) was calculated for each time point in the 500 ms pre-stimulus and the 500 ms during stimulus periods for all the electrodes. If >80% of all time points across the combined 1 s interval were found to have a significant phase-locking ($P < 0.005$), then the LFPs were considered to be synchronized in that trial. For bilateral recordings, the left and right hemispheres were analysed separately.

Phase-tightening. We calculated the Z-scores for LFP phases in 500ms pre-stimulus and 500ms during stimulus periods across all the electrodes in the recording array. If the Z-score was significantly higher (t test, $P<0.05$) in the during-stimulus period than in the pre-stimulus period then the phase was considered to be tightened. We used the percent change from the pre-stimulus to during-stimulus period to indicate the tightening of phase.

MUA synchronization. We measured synchronization in MUA data by counting the spikes within a brief time window (bin width, 2.5-10ms). This is similar to a peri-stimulus time

histogram (PSTH) over all MUA channels. In each trial we produced a PSTH over all the MUA channels and normalized it by the sum of the counts in all PSTH bins. If synchronization occurred in a certain time bin there should be a high spike count for that bin. Normalization was carried out to ensure that the influence of differential firing rates was removed. We then defined a MUA synchronization index as the sum of all the normalized spike counts which exceed half of the maximum value. We calculated the synchronization index choosing a bin width of 5 ms although we also used bin sizes of 2.5 ms and 10 ms and similar trends were observed.

The synchronization index was based on the following. Suppose that the total time T is divided into small time bins τ ($T/\tau = TN$), and that R spike trains are given by X_{ik} =0 (there is no spike) or 1 (there is at least one spike), i = 1,2,…,R, k =1, …, TN. We can then define:

$$Z_k = \frac{\sum_i X_{ik}}{\sum_{i=1}^{NR}\sum_{k=1}^{TN} X_{ik}},$$

If we then find those $Z_{k_l}, l = 1,\cdots,M$ (M<TN), that are larger than max(Z_k/2), then the synchronization index α can be defined as:

$$\alpha = \sum_{l=1}^{M} Z_{k_l} \Big/ M$$

Network model. We constructed an excitatory-inhibitory network comprising three populations of neurons: 100 excitatory (pyramidal) neurons, 50 inhibitory fast (inter) neurons and 50 inhibitory slow (inter)neurons. Similar models using fast and slow $GABA_A$ kinetics have been investigated for hippocampal neurons[27]. Here we focused on the network property in the visual discrimination tasks. Each set of neurons obeys the following integrate and fire equation:

$$\begin{cases} C_e \dfrac{dV_e^i}{dt} = -g_{eL}(V_e^i - V_{eL}) - I_{e,syn}^i + I_e^i + I_{app}^i, i = 1,\cdots,100 \\ C_I \dfrac{dV_{If}^j}{dt} = -g_{IL}(V_{If}^j - V_{IL}) - I_{If,syn}^j + I_{If}^j, j = 1,\cdots,50 \\ C_I \dfrac{dV_{Is}^k}{dt} = -g_{IL}(V_{Is}^k - V_{IL}) - I_{Is,syn}^k + I_{Is}^k, k = 1,\cdots,50 \end{cases}$$

where C_e, C_I are the capacitances for excitatory and inhibitory neurons, and I_e, I_{If} and I_{Is} represent the background currents for these three kinds of neurons, excitatory neurons(EX), fast inhibitory neurons (INf) and slow inhibitory neurons (INs). I_{app} is the external input. In the model, we assume that the initial conditions of all neurons are random and the connections are all-to-all. Each cell receives AMPA and NMDA receptor mediated currents from excitatory pyramidal cells, and $GABA_A$ receptor mediated currents from INf neurons and INs neurons. The only exception is that INs neurons do not receive inputs from INf ones. Thus the synaptic inputs have the following general forms:

$$\begin{cases} I_{e,syn}^i = I_{AMee}^i + I_{NMee}^i + I_{GAfe}^i + I_{GAse}^i \\ = \sum_{m=1}^{100} \bar{g}_{AMee} s_{AM}^m (V_E^i - E_e) + \sum_{m=1}^{100} \bar{g}_{NMee} B(V_E^i) s_{NM}^m (V_E^i - E_e) + \sum_{m=1}^{50} \bar{g}_{GAfe} s_{GAf}^m (V_E^i - E_I) + \sum_{m=1}^{50} \bar{g}_{GAse} s_{GAs}^m (V_E^i - E_I) \\ I_{if,syn}^J = I_{AMef}^j + I_{NMef}^j + I_{GAff}^j + I_{GAsf}^j \\ = \sum_{m=1}^{100} \bar{g}_{AMef} s_{AM}^m (V_E^j - E_e) + \sum_{m=1}^{100} \bar{g}_{NMef} B(V_{If}^j) s_{NM}^m (V_{If}^i - E_e) + \sum_{m=1}^{50} \bar{g}_{GAff} s_{GAf}^m (V_{If}^j - E_I) + \sum_{m=1}^{50} \bar{g}_{GAsf} s_{GAs}^m (V_{If}^i - E_I) \\ I_{Is,syn}^k = I_{AMes}^k + I_{NMes}^k + I_{GAss}^k \\ = \sum_{m=1}^{100} \bar{g}_{AMes} s_{AM}^m (V_{Is}^i - E_e) + \sum_{m=1}^{100} \bar{g}_{NMee} B(V_{Is}^i) s_{NM}^m (V_{Is}^i - E_e) + \sum_{m=1}^{50} \bar{g}_{GAse} s_{GAs}^m (V_E^i - E_I) \end{cases} \text{ii}$$

in which E_e, E_I are reverse potentials of excitatory and inhibitory neurons, respectively; $\bar{g}_{AMek}$, $\bar{g}_{NMek}$, $\bar{g}_{GAkl}$ $(k,l = e, f, s)$ are maximal channel conductances for AMPA, NMDA and $GABA_A$ receptors, respectively. An action potential is discharged when the membrane potential reaches a firing voltage threshold V_{th}. Then the membrane potential is reset to V_{reset}

and stays there for an absolute refractory period τ_{ref}. For EX cells, the parameters in the model are V_{th} = -52 mV, V_{reset} = -59 mV, τ_{ref} = 2ms, C_e = 0.5 nF, $\overline{g}_{eL}$ = 0.025 μS, V_{eL} = -70mV, the excitatory reverse potential E_e = 0 mV. For inhibitory cells, we set V_{th} = -52mV, V_{reset} = -60mV, V_{IL} = -65mV, C_I = 0.2 nF, $\overline{g}_{IL}$ =0.02 μS. The refractory time τ_{ref} = 1ms. The inhibitory reverse potential E_I = -70mV. The gating variables s_{AM}^m and s_{NM}^m are described by two first-order kinetics[28]:

$$\begin{cases} \dfrac{dx}{dt} = \alpha_{x,l} \sum_j \delta(t - t_j) - x / \tau_{x,l} \\ \dfrac{ds_l^m}{dt} = \alpha_{x,l} x(1 - s_l^m) - s_l^m / \tau_{x,l} \end{cases}$$

with $l = AM, NM$ where t_j is the presynaptic spike time. The channel parameters are α_x =1 ms^{-1}, τ_x =0.05 ms, α_s =1 ms^{-1}, τ_s =2 ms. The inhibitory postsynaptic current (IPSP) from slow and fast interneurons is mediated by the $GABA_A$ receptor. The gating variables $s_{GA,f}^m$ and $s_{GA,s}^m$ obey simple first-order kinetics (*S10*):

$$\frac{ds_{GA,l}^m}{dt} = \alpha_{II} \sum_j \delta(t - t_j^-)(1 - s_{GA,l}^m) - s_{GA,l}^m / \tau_{II}, l = f, s$$

Here the superscript in t_j^- indicates that the increment of $s_{GA,l}^m$ by a spike should be calculated using the value of $s_{GA,l}^m$ immediately before the spike on the right hand side of the equation:

$$\Delta s_{GA,l}^m = s_{GA,l}^m(t_j^+) - s_{GA,l}^m(t_j^-) = \alpha_I (1 - s_{GA,l}^m(t_j^-)), l = f, s$$

For the fast $GABA_A$ channel, we chose τ_{If} = 9 ms, and α_{If} = 1 ms^{-1}. For the slow $GABA_A$ channel, τ_{Is} = 50 ms, α_{Is} = 0.2 ms^{-1}. In the simulation spikes in all presynaptic neurons are connected to a convergent neuron. For the background current of EX cells, we set

$I_e^i = 0.7 + \xi_i(t), (i = 1, \cdots, 100)$ where $\xi_i(t)$ is white noise with $\sigma_e = 0.1$. For inhibitory cells, we set the background currents fixed and homogenous, for INf cells $I_{If}^j = 0.85, (j = 1, \cdots, 50)$ and for INs cells $I_{Is}^k = 0.6, (k = 1, \cdots, 50)$.

Parameters and analytical methods used in application of the model. To generate post learning effects the following coefficient values were used for the different sites of AMPA (AM), NMDA (NM) and $GABA_A$ (GA) receptors (e = excitatory neuron, s = slow inhibitory neuron and f = fast inhibitory neuron): AMee = 0.02; AMef = 0.08; AMes = 0.0005; NMee = 0.0035; NMef = 0.001; NMes = 0.00055; GAff & GAss = 0.08; GAfe = 0.015; GAse = 0.06; GAsf = 0.03. For pre-learning only the values of two NMDA receptor coefficients were reduced: NMee to 0.002 and NMes to 0.0001.

All the methods for calculating theta/gamma parameters were the same as for the data from IT recordings. For **Fig. 4** and the **Supplementary Figs. 2-5** data are from a single run of the model. For **Figs. 5 and 6** results are an average of 10 runs of the model.

ACKNOWLEDGEMENTS

This work was supported by a BBSRC grant and the Search Foundation (USA) (KK) and an EPSRC and EU grant (JF). We thank Andrew Tate and Andrea Leigh for their help with behavioural and recording experiments.

AUTHOR CONTRIBUTIONS

KMK designed the IT recording experiments and carried them out with HF and AUN. Data analysis was performed by YZ, AUN, HF and KMK. JF developed the neural network model

with contributions from XZ, YZ and KMK. Model simulations and analyses were performed by YZ and XZ. The paper was written by KMK, JF and YZ with technical contributions from XZ, HF and AUN..

1. Buzsaki, G. *Rhythms of the Brain* (Oxford University Press USA, 2006).
2. Lee, H., Simpson, G.V., Logothetis, N.K. & Rainer, G. Phase locking of single neuron activity to theta oscillations during working memory in monkey extrastriate visual cortex. *Neuron* **45**, 147-156 (2005).
3. Holscher, C., Anwyl, R. & Rowan, M.J. Stimulation on the positive phase of hippocampal theta Rhythm induces long-term potentiation that can be depotentiated by stimulation on the negative phase in area CA1 in vivo. *J. Neurosci.* **17**, 6470-6477 (1997).
4. Jensen, O., Kaiser, J. & Lachaux, J.P. Human gamma-frequency oscillations associated with attention and memory. *Trends Neurosci.*. **30**, 317-324 (2007).
5. Csibra, G., Davis, G., Spratling, M.W. & Johnson, M.H. Gamma Oscillations and Object Processing in the Infant Brain. *Science* **290**, 1582-1585 (2000).
6. Busch, N.A., Herrmann, C.S., Muller, M.M., Lenz, D. & Gruber, T. A cross-laboratory study of event-related gamma activity in a standard object recognition paradigm. *NeuroImage* **33**, 1169-1177 (2006).
7. Canolty, R.T., *et al.* High Gamma Power Is Phase-Locked to Theta Oscillations in Human Neocortex. *Science* **313**, 1626-1628 (2006).
8. Jensen, O. Maintenance of multiple working memory items by temporal segmentation. *Neuroscience* **139**, 237-249 (2006).
9. Fries, P., Reynolds, J.H., Rorie, A.E. & Desimone, R. Modulation of Oscillatory Neuronal Synchronization by Selective Visual Attention. *Science* **291**, 1560-1563 (2001).
10. Fries, P. A mechanism for cognitive dynamics: neuronal communication through neuronal coherence. *Trends Cog. Sci.* **9**, 474-480 (2005).
11. Rizzuto, D.S., *et al.* Reset of human neocortical oscillations during a working memory task. *Proc. Natl. Acad. Sci. USA.* **100**, 7931-7936 (2003).
12. Sederberg, P.B., Kahana, M.J., Howard, M.W., Donner, E.J. & Madsen, J.R. Theta and Gamma Oscillations during Encoding Predict Subsequent Recall. *J. Neurosci.* **23**, 10809-10814 (2003).

13. Lakatos, P., *et al.* An oscillatory hierarchy controlling neuronal excitability and stimulus processing in the auditory cortex. *J. Neurophysiol.* **94**, 1904-1911 (2005).
14. Tate, A.J., Fischer, H., Leigh, A.E. & Kendrick, K.M. Behavioural and neurophysiological evidence for face identity and face emotion processing in animals. *Phil. Trans.Roy. Soc. B: Biol. Sci.* **361**, 2155-2172 (2006).
15. White, J.A., Banks, M.I., Pearce, R.A. & Kopell, N.J. Networks of interneurons with fast and slow Î³-aminobutyric acid type A (GABAA) kinetics provide substrate for mixed gamma-theta rhythm. *Proc. Natl. Acad. Sci. USA.* **97**, 8128-8133 (2000).
16. Tort, A.B.L., et al., On the formation of gamma-coherent cell assemblies by oriens lacunosum-moleculare interneurons in the hippocampus. *Proc. Natl. Acad. Sci. USA.* **104**, 13490-13495 (2007)
17. Sceniak M.P. & MacIver M.B. Slow $GABA_A$ mediated synaptic transmission in rat visual cortex. *BMC Neurosci*. **9,** 1-14 (2008).
18. Pearce R.A. Physiological evidence for two distinct $GABA_A$ responses in rat hippocampus. *Neuron* 10, 189-200 (1993)
19. Rolls, E.T., Judge, S.J. & Sanghera, M.J. Activity in the inferotemporal cortex of the alert monkey. *Brain Res.* **130,** 229-238.
20. Liu, L., *et al.* Role of NMDA Receptor Subtypes in Governing the Direction of Hippocampal Synaptic Plasticity. *Science* **304**, 1021-1024 (2004).
21. Smith, M.A. & Kohn A. spatial and temporal scales of neuronal correlation in primary visual cortex. *J. Neurosci.* **28,** 12591-12603 (2008)
22. Kendrick, K.M. & Baldwin, B.A. in *Methods in Neuroscience* (ed. P.M. CONN) 3-15 (Academic Press, New York, 1991).
23. Horton, P.M., Nicol, A.U., Kendrick, K.M. & Feng, J.F. Spike sorting based upon machine learning algorithms (SOMA). *J. Neurosci. Meth.* **160**, 52-68 (2007).
24. Torrence, C. & Compo, G.P. A Practical Guide to Wavelet Analysis. *Bull. Am. Met. Soc.* **79**, 61-78 (1998).
25. Fisher, N.I. Statistical analysis of circular data. (Cambridge University Press, Cambridge, 1993)
26. Halliday, D.M., *et al.* A framework for the analysis of mixed time series/point process data--Theory and application to the study of physiological tremor, single motor unit discharges and electromyograms. *Prog. Biophys. Mol. Biol.* **64**, 237-278 (1995).

27. Wang, X.-J. Synaptic Basis of Cortical persistent activity: the importance of NMDA receptors to working memory. *J. Neurosci.* **19**, 9587-9603 (1999).
28. Wang, X.-J. & Rinzel, J. Alternating and Synchronous Rhythms in Reciprocally Inhibitory Model Neurons. *Neural Comp.* **4**, 84-97 (1992).

Figure 1. Theta/gamma coupling in IT and in simulations. (**a**) Typical examples of coupling between theta phase and gamma amplitude in three animals for the pre-stimulus (left) and during-stimulus (right) periods (from top to bottom, sheep A session 071004-1 channel 2, sheep B session 110305-1 channel 3, sheep C session 230305-2 channel 75) before (left) and during (right) presentation of a learned stimulus pair. There is a clear increase in coherence across the ranges of both frequencies during the stimulus. The red/yellow contour lines indicate significance changes ($P<0.001$). (**b**) Theta phase/gamma amplitude coupling using simulation data (top two panels). 50 Hz sine waves were nested on top of 5 Hz sine waves with peak ratio 1:5. In the pre-stimulus period the amplitude of the sine wave is 1/3 of the one in the during-stimulus period. The bottom left panel shows the simulation using i) Complete sets of two cycles of 50 Hz waves inserted into the same phase of each 5 Hz wave cycle (blue). ii) Complete set of 50 Hz wave were inserted into the random phase of each 5 Hz cycle (red). iii) Incomplete set of 50 Hz were inserted into the random phase of 5 Hz cycles in which not every 5 Hz cycle had 50 Hz waves on it.

Figure 2 Evoked potential, MUA and theta latency profiles and theta/gamma activity changes after learning (**a**) Typical average latency profile for theta, MUA and VEP (P100 and N300) over 40 trials post learning (face-pair shown at time 0). (**b**) Mean ± sem % change in theta amplitude (**c)** Gamma amplitude (**d**) Theta/gamma ratio (**e**) Theta gamma coherence and (**f**) Theta phase tightening (**g**) Mean ± sem z-scores for theta phase synchronization and (**h**) Theta phase reset in the right and left IT of the 3 different animals (A,B and C) during sessions where discrimination learning performance had yet to reach >80% criterion (NL, mean±sem correct % Sheep A = 57.5±3.2%, Sheep B = 57.1±7.6%, Sheep C= 67±4.5%) compared with those where it had (L, Sheep A=89.4±3.1% – $P<0.001$, Sheep B=85.7±4% – $P=0.001$, Sheep C=90.5±2.5% – $P=0.002$). *$P<0.05$, **$P<0.01$, ***$P<0.001$ vs NL and #$P<0.05$, ##$P<0.01$, ###$P<0.001$ vs right hemisphere. Overall mean ±sem pre-stimulus values across the 3 animals were: Theta amplitude (mV) Right 5.33±0.4, Left 6.99±0.37; gamma amplitude (mV) Right 1.75±0.19, Left 2.87±0.17; Theta/gamma ratio Right 3.41±0.18, Left 2.95±0.13; Theta/gamma coherence Right 0.13±0.01, Left 0.128±0.01; Theta phase tightening Right z=37.3±1.85, Left 24.9±2.08.

Figure 3. Rapid time course of learning effects on theta nested gamma. Pseudocolor panels show changes in: (**a**) Theta amplitude, (**b**) Theta/gamma ratio and (**c**) Coherence between theta phase and gamma amplitude in the right IT during the learning of one new face pair in Sheep B over sequential (top to bottom) blocks of 20-40 trials conducted over approximately 20 min (data plotted from 60 electrodes). Discrimination performance across the 4 blocks was 70%, 93%, 90% and 90% correct respectively (i.e. the learning criterion of >80% was achieved in the second and subsequent blocks). The face pair stimulus occurs at time zero and the pseudocolor scale indicates normalised (by the maximum value during the stimulus) differences between pre and during stimulus.

Figure 4. Neural network model showing effects of altering theta and gamma contributions (**a**) Schematic showing connectivity in the neural network model together with the coefficient variables representing AMPA (AM), NMDA (NM) and GABA $_A$ (GA) receptors (IN(s) = slow and IN(f) = fast inhibitory neuron, Ex (e) = excitatory neuron (**b**) Responses to both a ramped and white noise stimulus (top. I_{app} = 0.8) made by excitatory neurons, LFP, the power contribution of different frequencies across the theta/gamma range, the downstream neuron and coupling of theta phase and gamma amplitude. Left column is with shallow nested gamma as seen in IT recordings following learning. Data are from a single run of the model (AMee = 0.02; AMef = 0.08; AMes = 0.0005; NMee = 0.0035; NMef = 0.001; NMes = 0.00055; GAff & GAss = 0.08; GAfe = 0.015; GAse = 0.06; GAsf = 0.03 – theta/gamma ratio = 3.4:1 , middle is with deep nested gamma (GAfe = 0.045 – theta/gamma ratio = 2.7:1) and right is with minimal gamma (GAse and GAsf = 0.12 theta/gamma ratio = 10:1).

Figure 5. Learning effects produced by the model (after learning = black; before learning = gray) by altering NMDA receptor sensitivity alone (NMee and NMes see **Fig 4a**). Graphs show changes in (**a**) Theta and gamma amplitude as a function of stimulus strength (I_{app}). (**b**) Theta/gamma ratio, (**c**) Coherence between theta phase and gamma amplitude (**d**) Firing rate of the excitatory output neurons (**e**) Firing rate of the downstream neuron and (**f**) Positive correlation between firing rate of the downstream neuron and the magnitude of the theta/gamma ratio ($r = 0.34$, $P<0.01$). NMDA, AMPA and $GABA_A$ receptor coefficients for after learning are the same as for shallow nested gamma in **Fig. 4b**. For before learning NMee = 0.002; NMes = 0.0001. Data are means±sem from 10 averaged runs of the model. Taking an overall average across the different values of Iapp, t-tests revealed significant differences between before and after learning – theta amplitude (**a**), $t^{18} = 81.5$, $P<0.0001$; gamma amplitude (**a**), $t^{18} = -12.1$, $P<0.0001$; theta/gamma ratio (**b**), $t^{18} = 32.02$, $P<0.0001$; theta/gamma coherence (**c**), $t^{18} = 2.6$, $P = 0.03$; excitatory neuron firing rate (**d**), $t^{18} = -2.23$, $P = 0.04$ and the firing rate of the downstream neuron (**e**), $t^{18} = 13.6$, $P<0.0001$.

Figure 6. Learning-associated desynchronization in model excitatory neurones and IT. Graphs show (**a**) Significantly greater desynchronization of the 100 excitatory neurons in the model as a function of stimulus strength (Iapp) after learning (black) compared with during it (grey) (using an overall mean for all Iapp values $t^{18} = -5.30$, $P<0.0001$). Data are mean±sem from 10 runs (**b**) Negative correlation between synchronization index and firing rate of the downstream neuron $r = -0.60$, $P<0.001$ (**c**) Negative correlation between excitatory neuron synchronization and size of the theta/gamma ratio, $r = -0.42$, $P<0.001$, (**c**) Negative correlation between synchronization and the theta/gamma ratio in MUA recordings from IT ($r = -0.3$, $P<0.001$), (**e**) Firing frequency distribution and theta waves generated by the model's 100 excitatory neurons in 5ms bins for 1s after stimulus onset during learning and (**f**) after learning (Iapp = 0.8). After learning more time bins during theta waves have active neurons compared with before learning as a result of greater desynchronization. NMDA, AMPA and $GABA_A$ receptor coefficients as in **Fig. 5**.

a

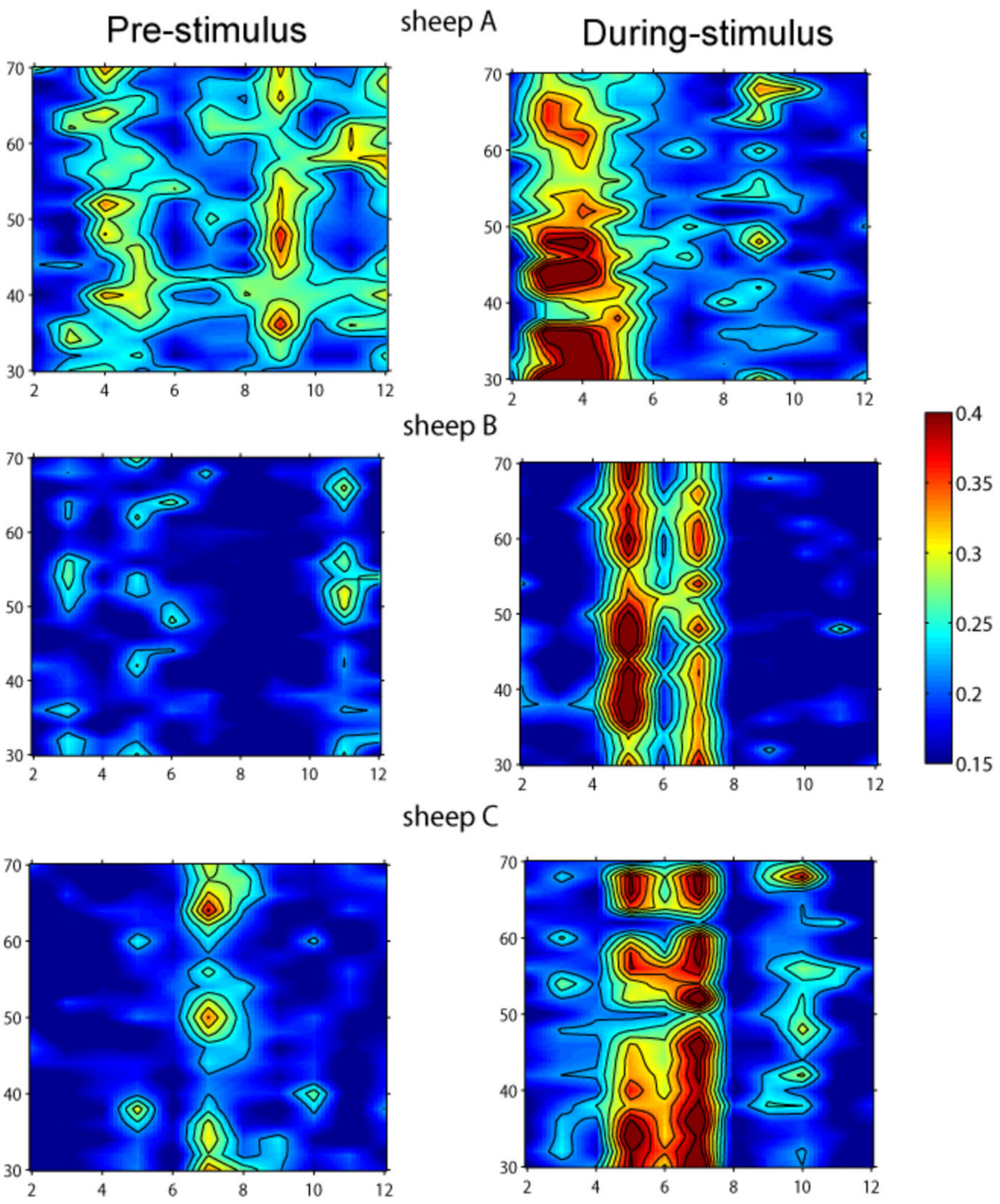
Pre-stimulus
During-stimulus
sheep A
sheep B
sheep C
70
60
50
40
30
2
4
6
8
10
12
0.4
0.35
0.3
0.25
0.2
0.15

b

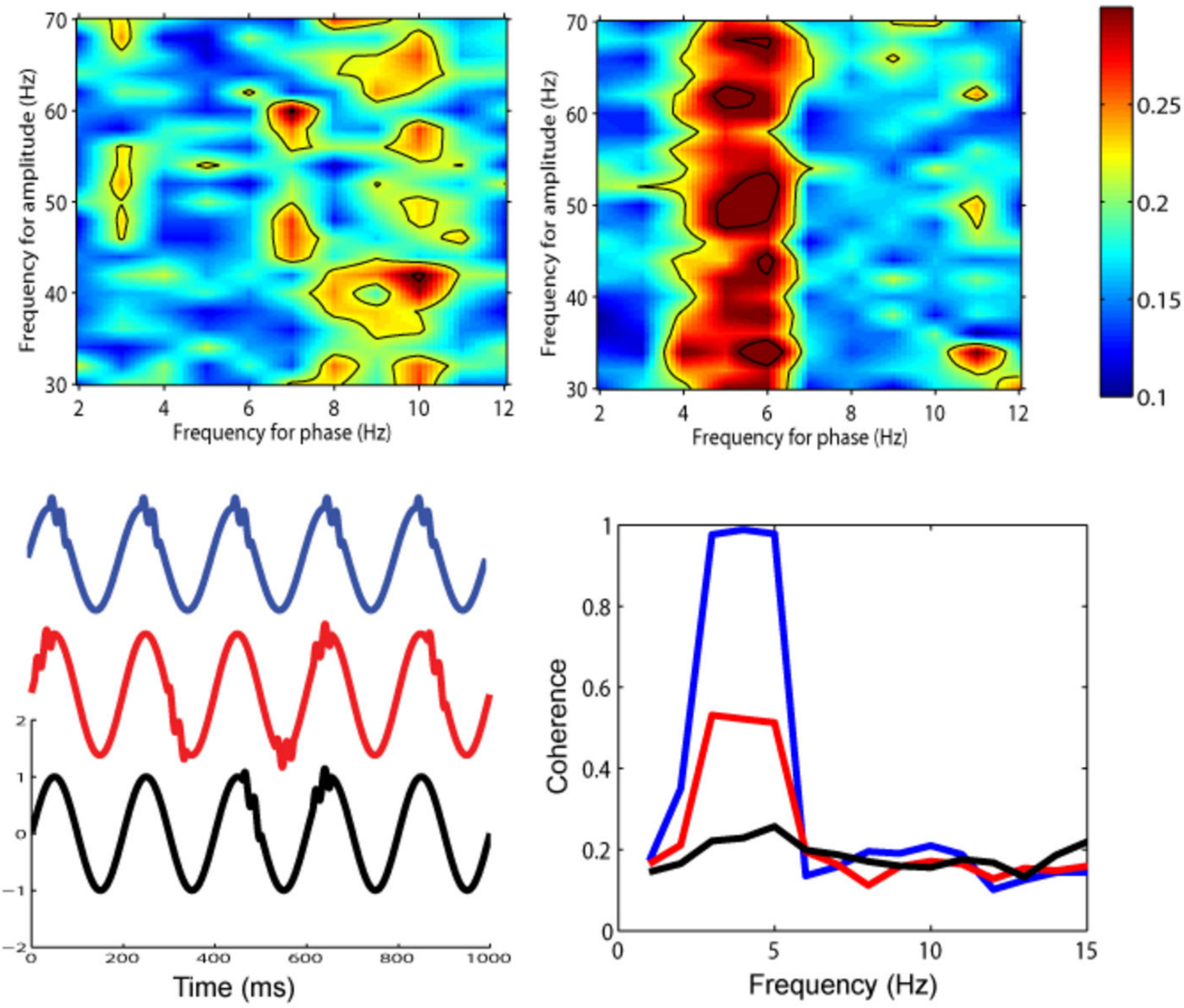
Frequency for amplitude (Hz)
Frequency for phase (Hz)
0.25
0.2
0.15
0.1
Time (ms)
Coherence
Frequency (Hz)

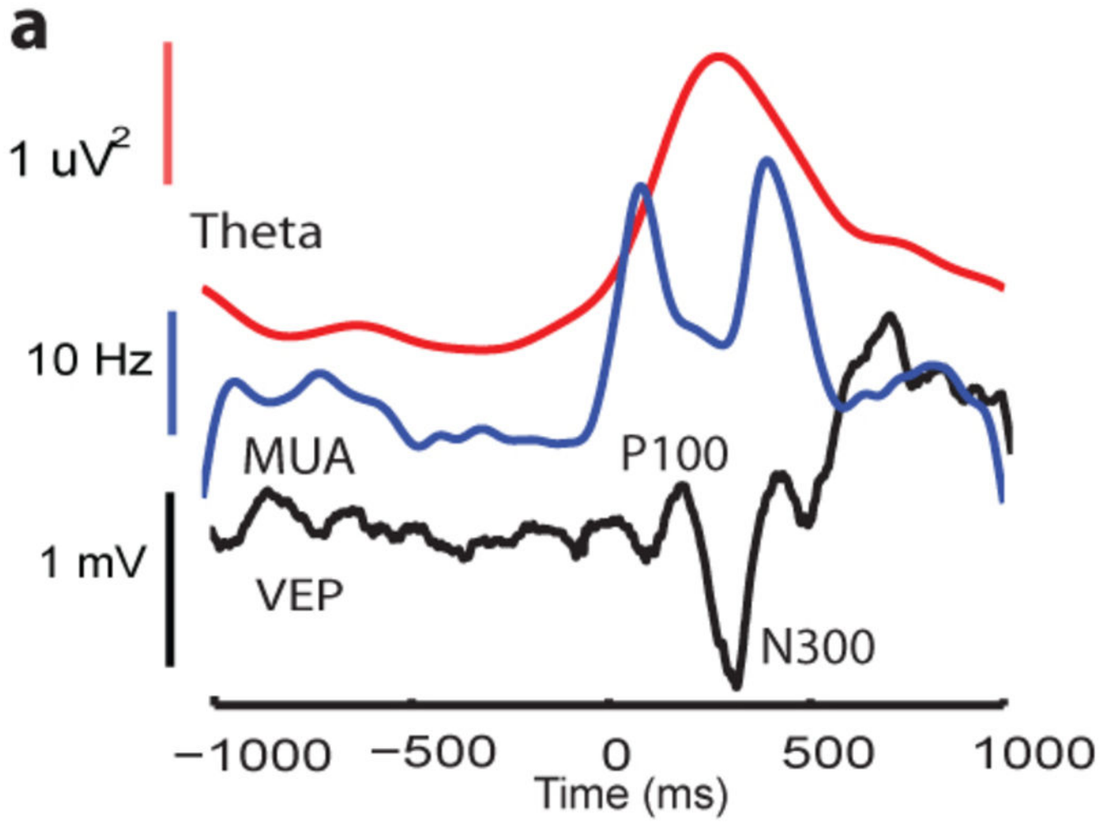
a
1 uV²
Theta
10 Hz
MUA
P100
1 mV
VEP
N300
−1000
−500
0
500
1000
Time (ms)

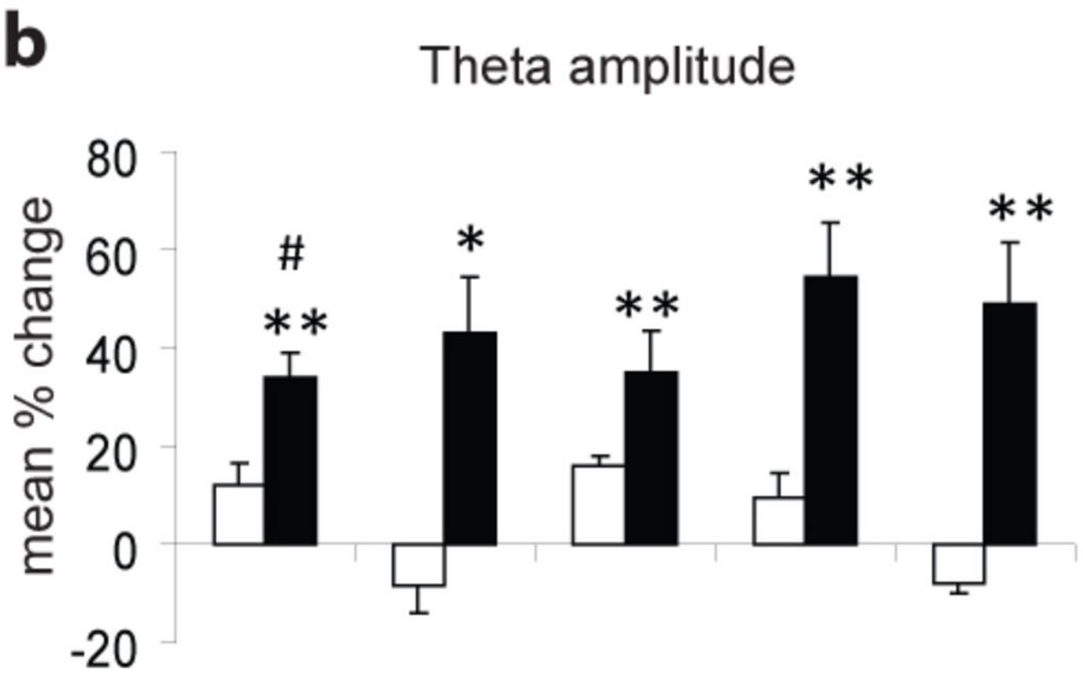
b
Theta amplitude
mean % change
80
60
40
20
0
-20
#
**
*
**
**
**

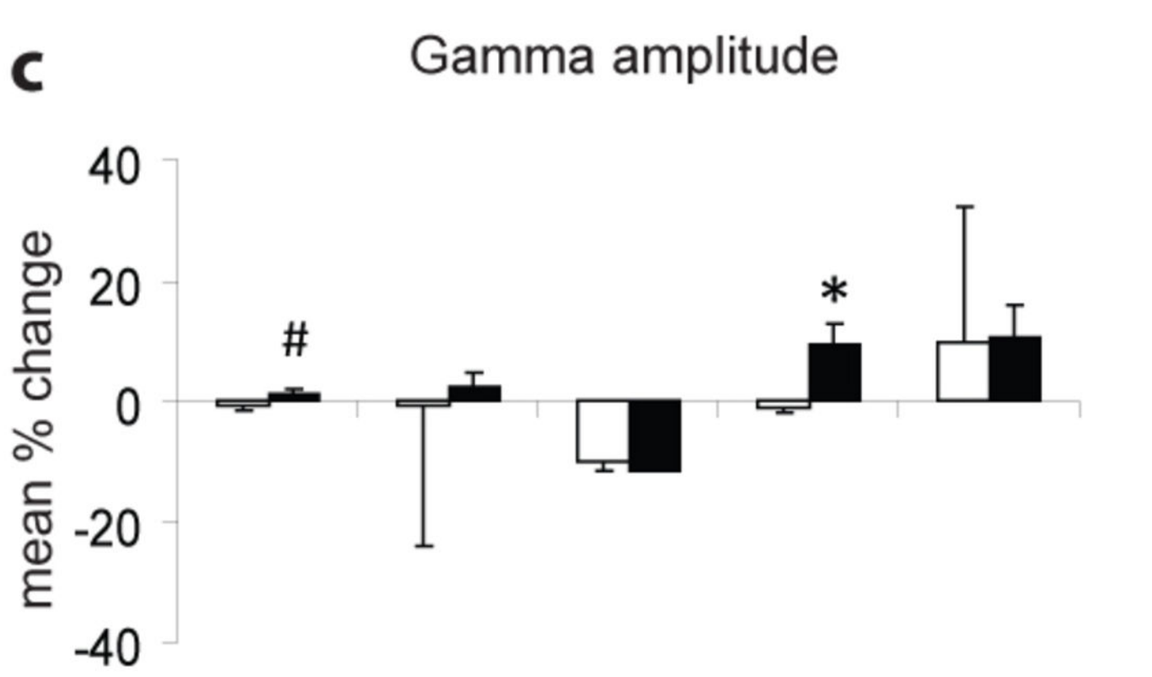
c
Gamma amplitude
mean % change
40
20
0
-20
-40
#
*

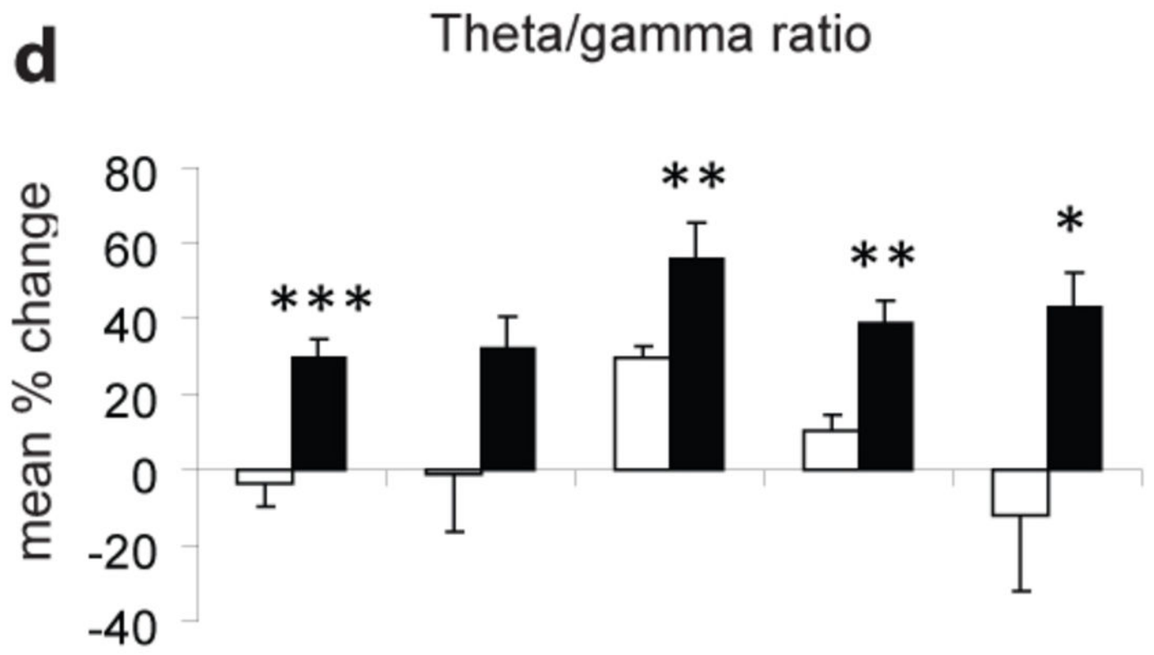
d
Theta/gamma ratio
mean % change
80
60
40
20
0
-20
-40
***
**
**
*

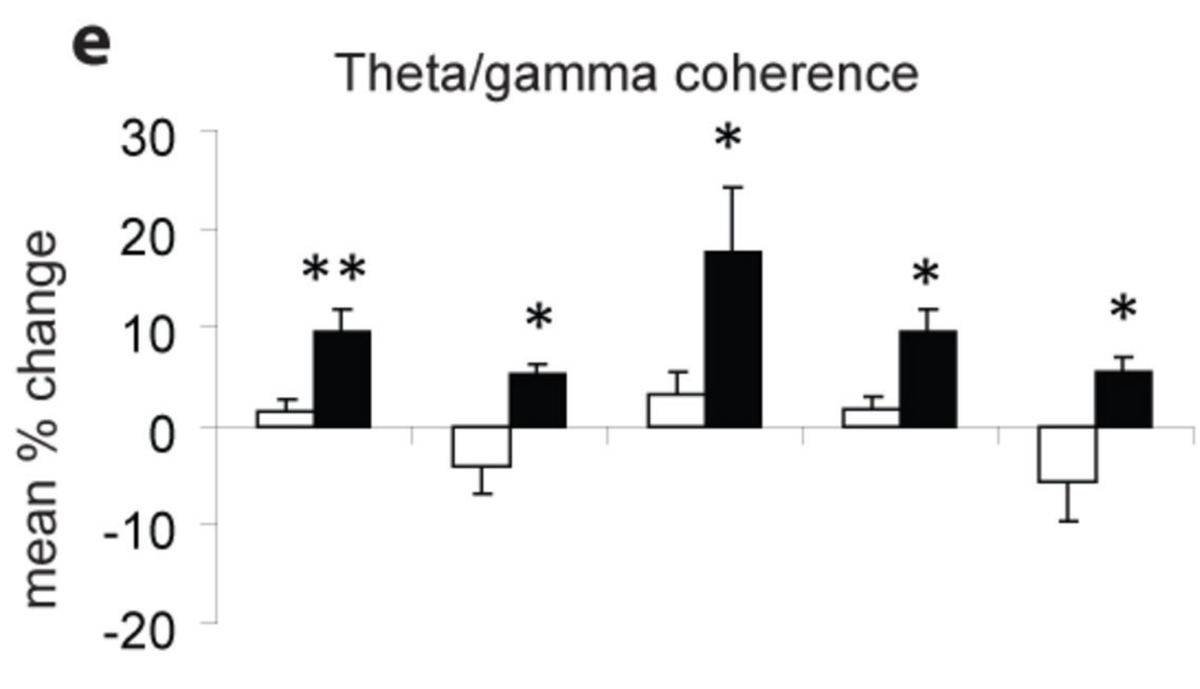
e
Theta/gamma coherence
mean % change
30
20
10
0
-10
-20
**
*
*
*
*

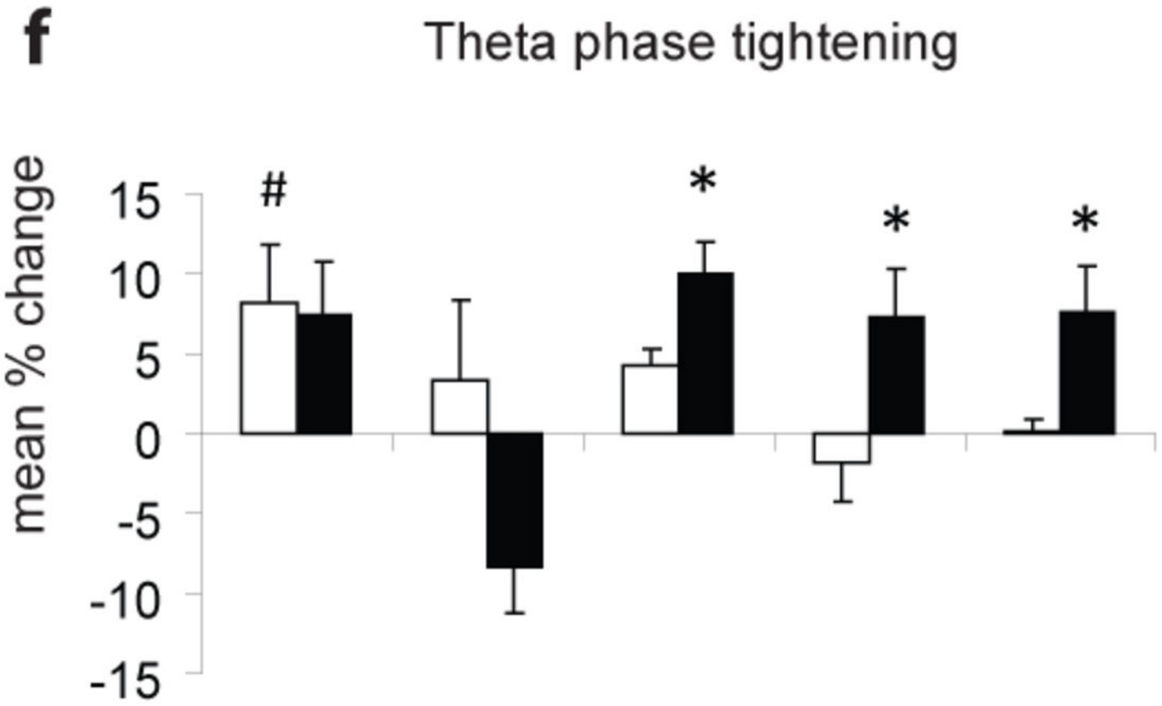
f
Theta phase tightening
mean % change
15
10
5
0
-5
-10
-15
#
*
*
*

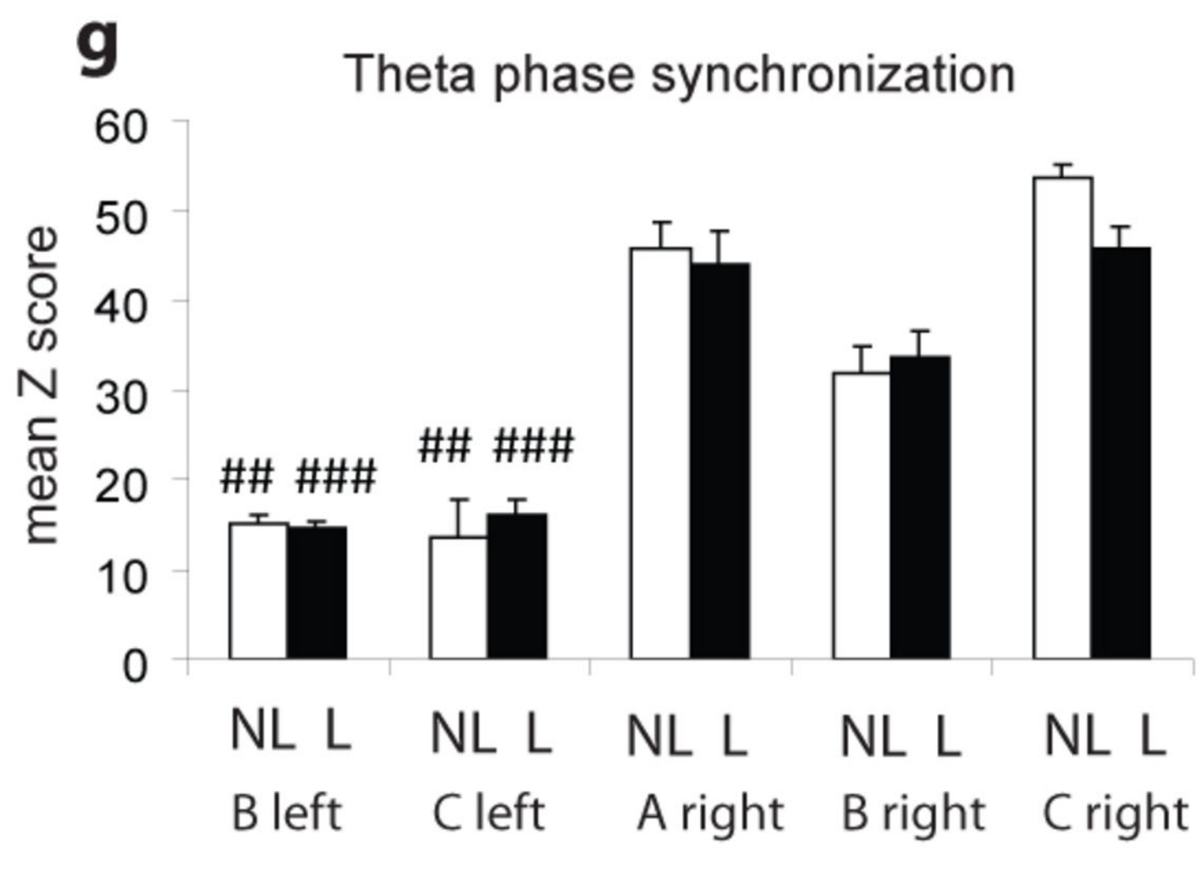
g
Theta phase synchronization
mean Z score
60
50
40
30
20
10
0
###
###
NL L
B left
C left
A right
B right
C right

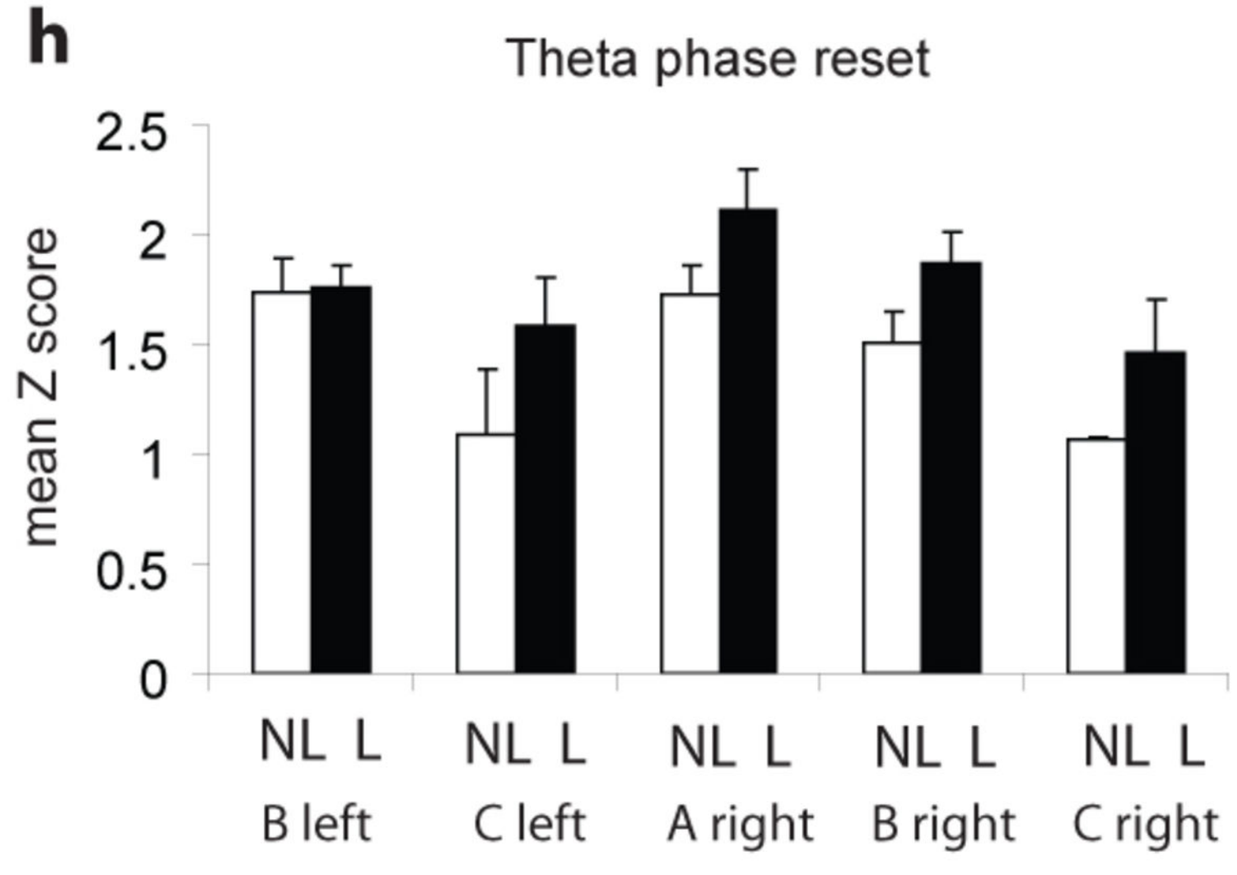
h
Theta phase reset
mean Z score
2.5
2
1.5
1
0.5
0
NL L
B left
C left
A right
B right
C right

a

b

c

0.5

0

6

0

0.2

0

Electrode no.

20

40

60

–400 –200 0 200 400

Time (ms)

Electrode no.

20

40

60

–400 –200 0 200 400

Time (ms)

Frequency for gamma amplitude (Hz)

60

40

2 4 6 8 10

Frequency for theta phase (Hz)

a

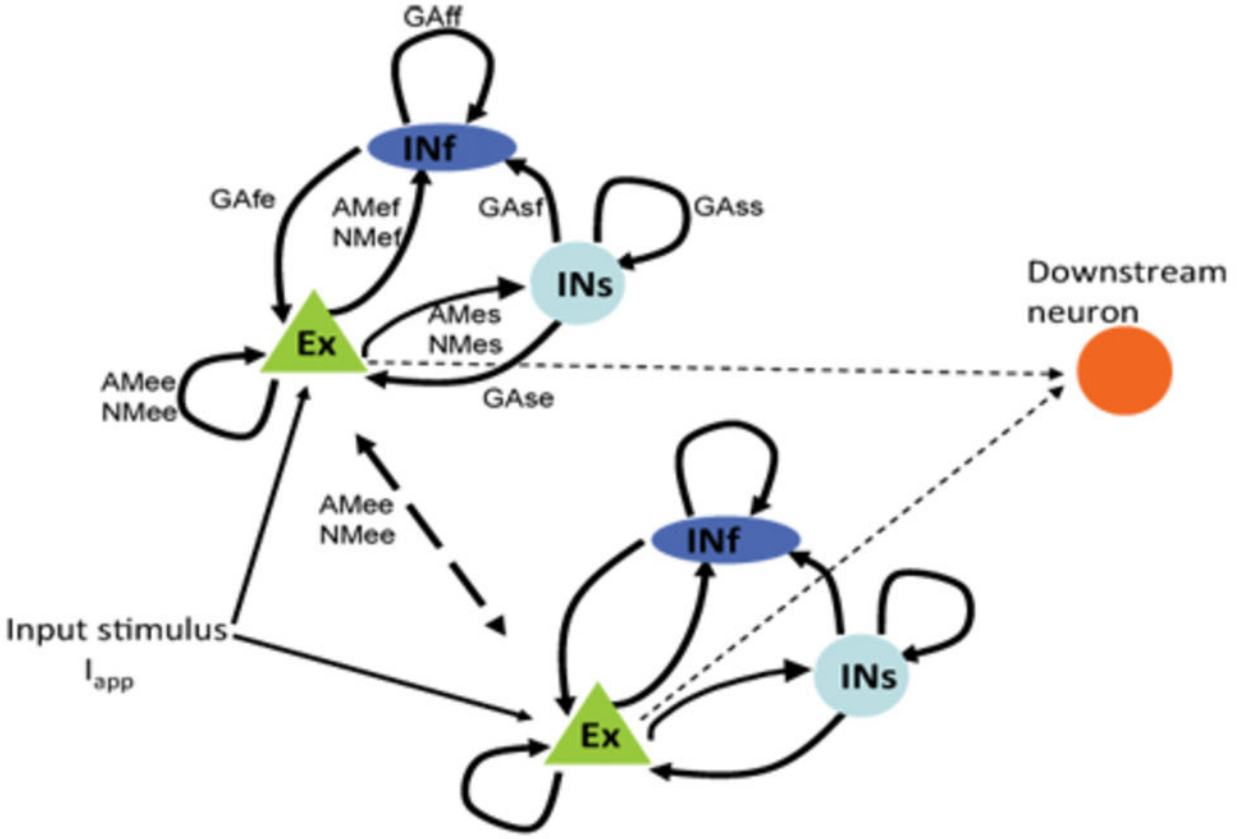
GAff
INf
GAfe
AMef
NMef
GAsf
GAss
INs
Ex
AMes
NMes
GAse
AMee
NMee
Downstream
neuron
AMee
NMee
INf
Input stimulus
I_{app}
INs
Ex

b

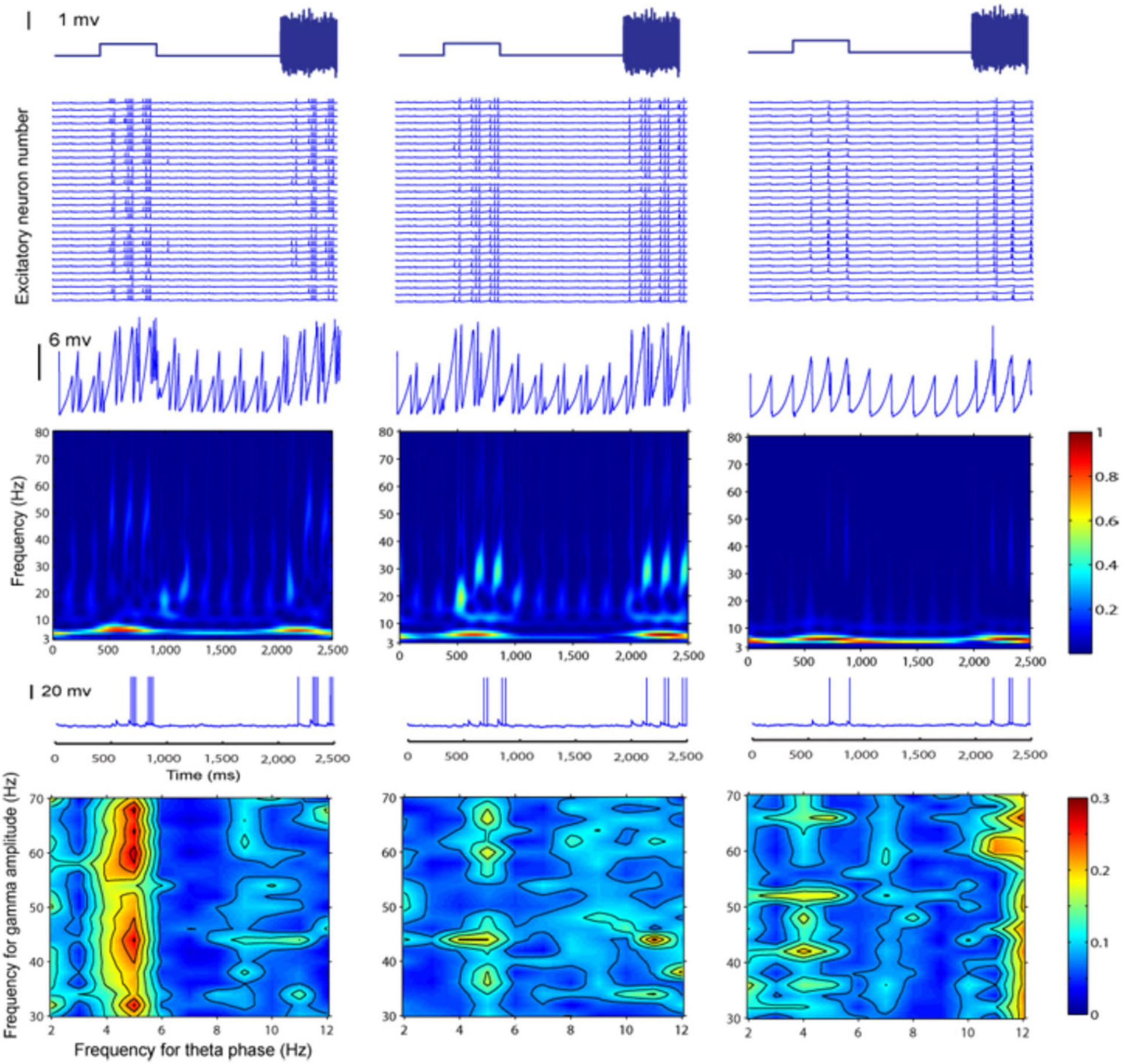
1 mv
Excitatory neuron number
6 mv
Frequency (Hz)
20 mv
Time (ms)
Frequency for gamma amplitude (Hz)
Frequency for theta phase (Hz)

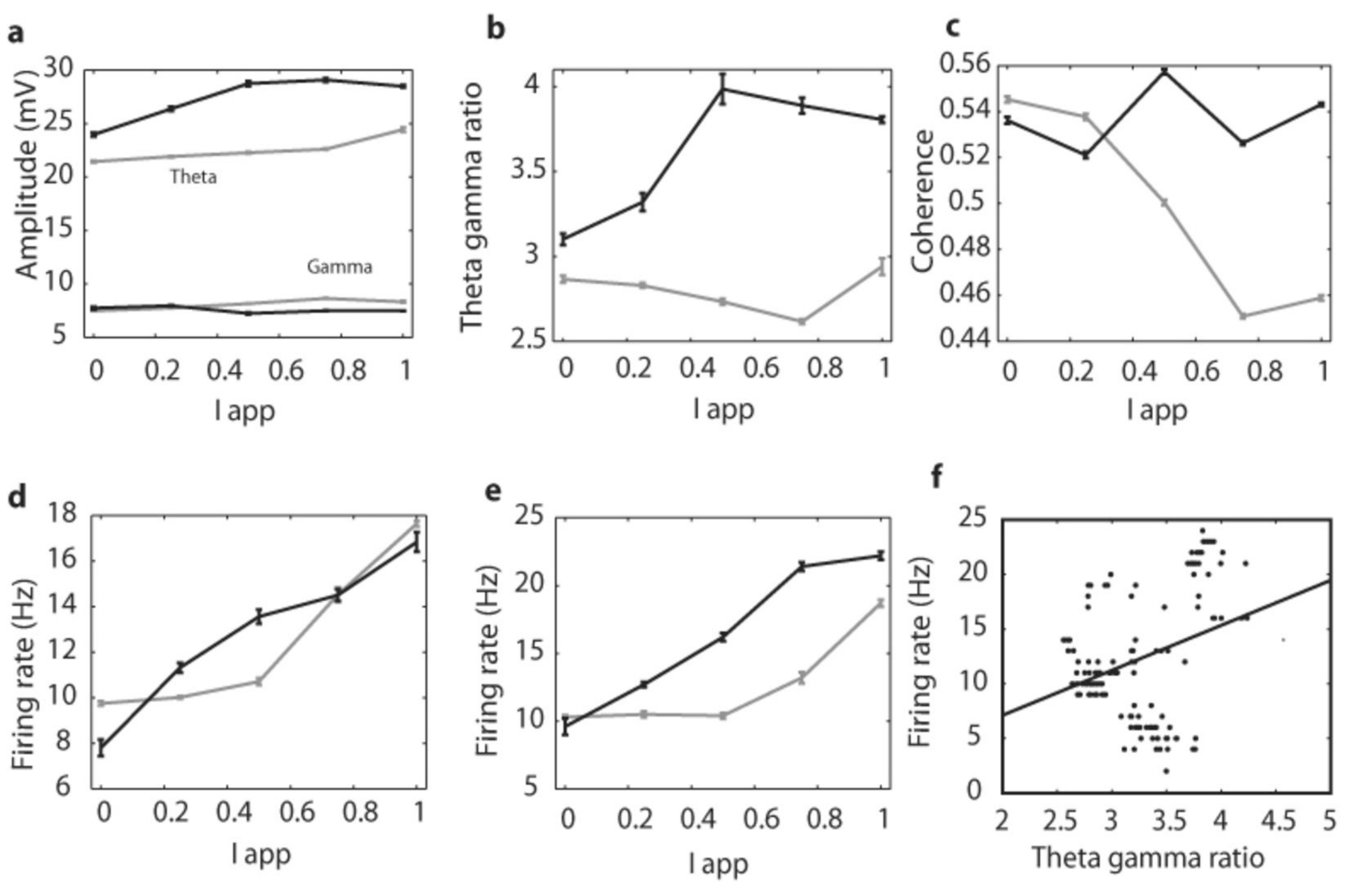
a
Amplitude (mV)
30
25
20
15
10
5
Theta
Gamma
0
0.2
0.4
0.6
0.8
1
I app
b
Theta gamma ratio
4
3.5
3
2.5
0
0.2
0.4
0.6
0.8
1
I app
c
Coherence
0.56
0.54
0.52
0.5
0.48
0.46
0.44
0
0.2
0.4
0.6
0.8
1
I app
d
Firing rate (Hz)
18
16
14
12
10
8
6
0
0.2
0.4
0.6
0.8
1
I app
e
Firing rate (Hz)
25
20
15
10
5
0
0.2
0.4
0.6
0.8
1
I app
f
Firing rate (Hz)
25
20
15
10
5
0
2
2.5
3
3.5
4
4.5
5
Theta gamma ratio

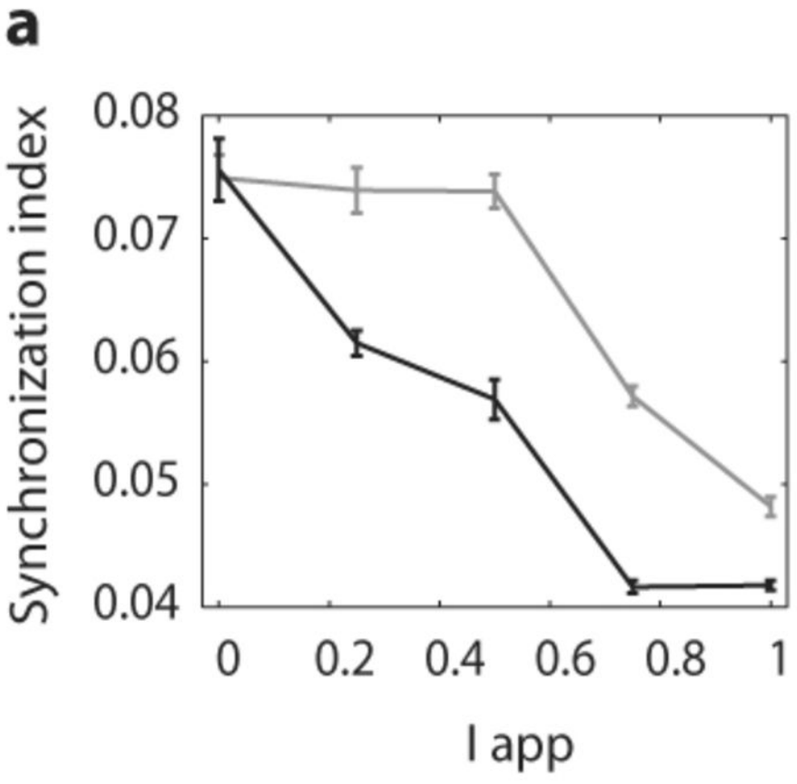
a
Synchronization index
0.08
0.07
0.06
0.05
0.04
0
0.2
0.4
0.6
0.8
1
I app

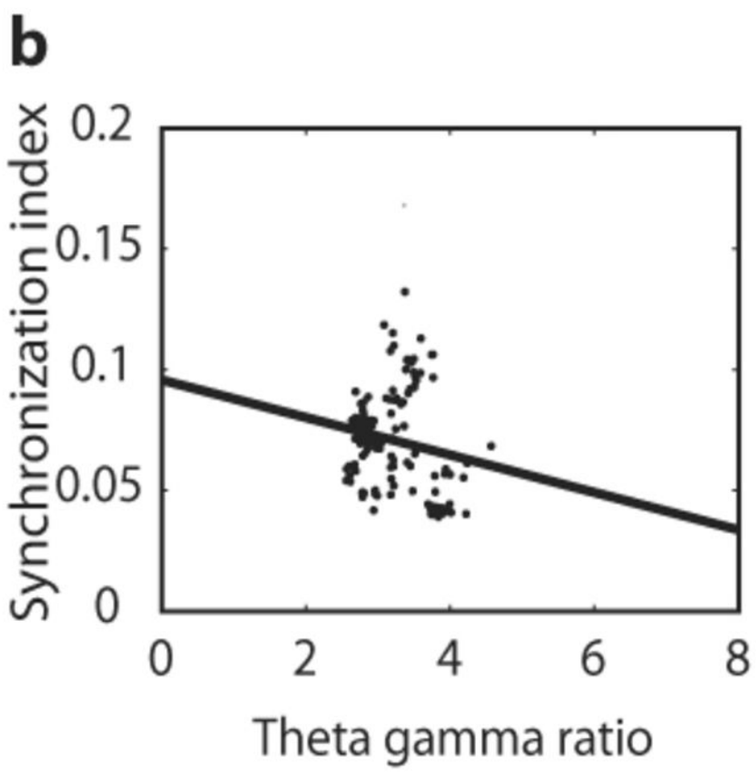
b
Synchronization index
0.2
0.15
0.1
0.05
0
0
2
4
6
8
Theta gamma ratio

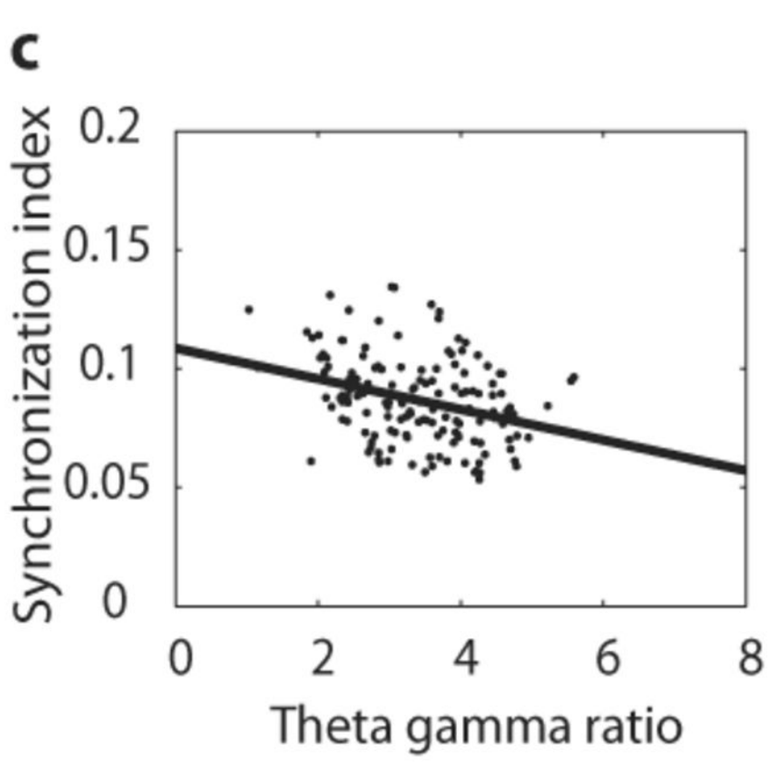
c
Synchronization index
0.2
0.15
0.1
0.05
0
0
2
4
6
8
Theta gamma ratio

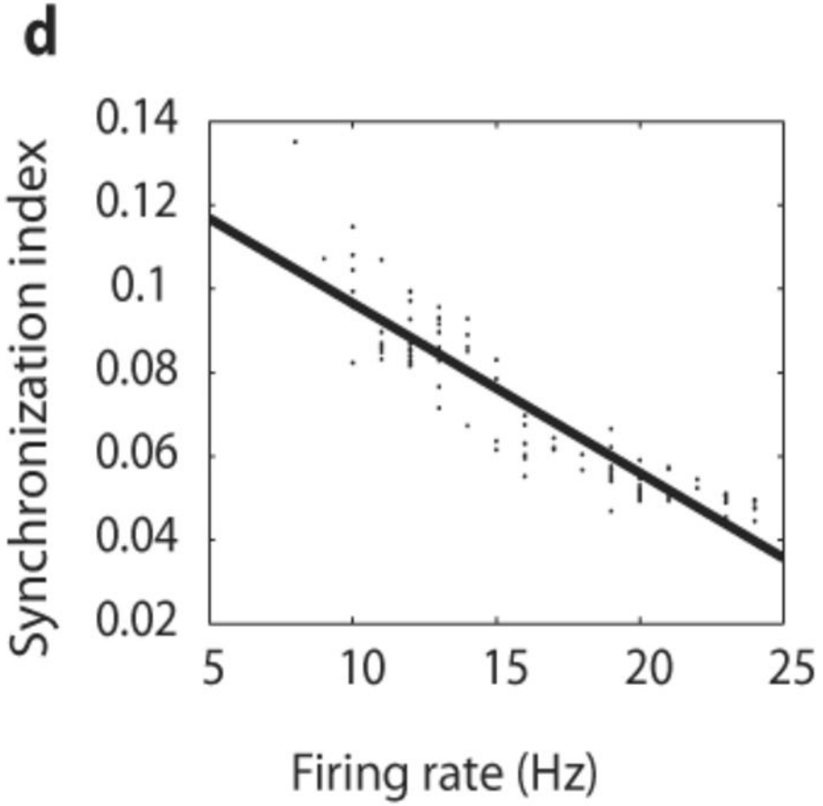
d
Synchronization index
0.14
0.12
0.1
0.08
0.06
0.04
0.02
5
10
15
20
25
Firing rate (Hz)

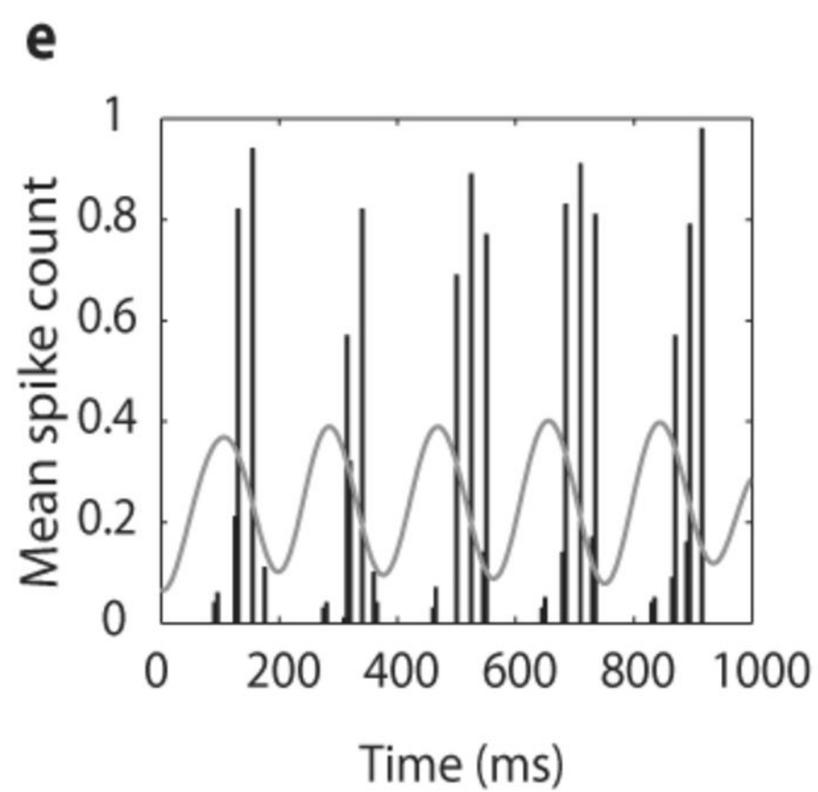
e
Mean spike count
1
0.8
0.6
0.4
0.2
0
0
200
400
600
800
1000
Time (ms)

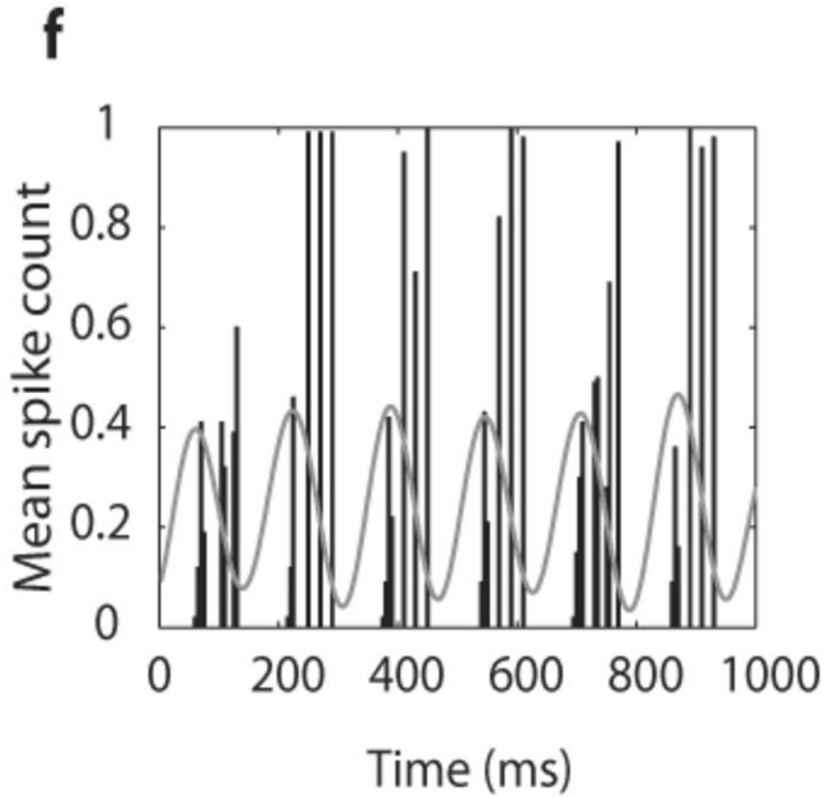
f
Mean spike count
1
0.8
0.6
0.4
0.2
0
0
200
400
600
800
1000
Time (ms)